[AMERICAN JOURNAL OF SCIENCE, VOL. 292, JANUARY, 1992, P. 21–57]

EXPERIMENTAL INVESTIGATION OF MASS TRANSFER—ALBITE, CaAl-SILICATES, AND AQUEOUS SOLUTIONS

NICHOLAS M. ROSE*, DENNIS K. BIRD, and J. G. LIOU
Department of Geology, Stanford University, Stanford, California 94305

ABSTRACT. Fluid-mineral experiments have been combined with theoretical mass transfer models to examine the geochemical evolution of hydrothermal pore fluids under conditions where albite is replaced by CaAl-silicates. This mineral paragenesis is commonly observed within high permeability zones in gabbros, diabases, and basalts. Experiments at 300°C and 300 bars reacted albite, prehnite, and quartz with dilute aqueous solutions; the initial solution compositions and proportions of reactant minerals allowed for rapid saturation with quartz, prehnite, and wairakite but continued irreversible dissolution of albite. The experimental solutions were incrementally sampled to obtain trends in solution chemistry that were correlated with the textures of reactant and secondary phases and compared with the theoretical models.

There was close agreement between theoretically predicted and experimentally observed trends. Both approaches illustrate systematic changes in solution chemistry during the dissolution of albite and formation of CaAl-silicates characterized by: (1) An early short-lived episode that precedes saturation with quartz and CaAl-silicates (prehnite and wairakite) characterized by a maxima in Al concentration and an increase in pH. (2) A stage where fluid chemistry is controlled by Na release to the fluid due to albite hydrolysis and Ca-removal from the fluid due to wairakite precipitation. During this stage one mole of Ca is removed from solution for every two moles of Na added; pH and Al concentrations are approximately constant. (3) A late stage, close to albite equilibrium, characterized by a rapid increase in pH and Al concentration, and a near constant Ca concentration. Discontinuities in the derivatives of solute concentration and pH with respect to reaction progress occur early in the reaction as the solution becomes saturated with prehnite, wairakite, and quartz. Large variations in these same derivatives occur later in the reaction and are controlled by electroneutrality requirements that reflect the speciation of Ca, Na, and Al in solution.

The calculations and experimental results suggest that the presence of secondary albite or of albite as a component in primary plagioclase may provide the chemical driving force for extreme Ca-metasomatism of gabbros, diabases, and basalts. Ca-metasomatism may be enhanced in response to fluids moving through temperature and pressure gradients that lead to albite undersaturation. In particular, calculations of Ca-solubility buffered by albite and CaAl-silicates indicate that these conditions will occur during fluid flow along positive temperature gradients.

* Present address: Geologisk Museum, Øster Voldgade 5-7, 1350 København K, Denmark.

INTRODUCTION

Calcium metasomatism, during which mafic rocks are replaced by prehnite-, epidote- or zeolite-rich assemblages, is a common feature observed in ophiolites and oceanic crust (Balsillie, 1932; Richardson and others, 1987; Schiffman and others, 1987; Harper, Bowman, and Kuhns, 1988). This includes altered basalts, gabbros, and diabase dikes from the East Greenland Tertiary igneous province (Rose and Bird, 1987; Bird, Manning, and Rose, 1988). Extreme calcium metasomatism, such as the epidosites found in ophiolites or prehnite mineralized dikes in East Greenland, is restricted to zones indicative of high rock permeability and large time-integrated fluid fluxes. Mineral paragenesis accompanying Ca-metasomatism is characterized by replacement of hydrothermal albite by secondary CaAl-silicates including epidote and prehnite. This paragenesis and related bulk chemical changes suggest that a simple relation exists between the metasomatic replacement of albite by CaAl-silicates and the Na and Ca concentrations in coexisting pore fluids. To better understand this relationship, we have combined experimental observations with theoretical modelling of the irreversible hydrolysis of albite in the system Na_2O–CaO–Al_2O_3–SiO_2–H_2O–HCl.

The experiments are closed system isothermal reactions run in large volume apparatus with facilities for in situ sampling (Seyfried, Janecky, and Berndt, 1987). They are ideally suited for comparison with predictive reaction path models (Helgeson, 1968, 1979; Helgeson and others, 1970). The reaction path is defined here as the evolution of fluid chemistry and extent of precipitation or dissolution of secondary phases during irreversible dissolution of one or more reactants. Reaction path models were used to optimize experimental conditions for elemental mass transfer during the irreversible hydrolysis of albite and to evaluate experimental data in terms of local equilibrium constraints on the transfer of elements between aqueous solutions and the reactant and product minerals. The accuracy of theoretical reaction path models is tested by experimental studies of simple systems in which cause and effect relations between the evolution of fluid composition and possible mineral dissolution or precipitation reactions can be understood. The closed system isothermal experimental and theoretical models provide a basis for evaluating more complex behavior of open systems in the presence of pressure and temperature gradients.

Ca-metasomatism in basaltic systems.—Regional metamorphism of basaltic rocks at temperatures between 250° and 400°C and at pressures below 1 kb produces mineral assemblages of albite + epidote + chlorite ± actinolite ± oxides (greenschist facies) or albite + epidote + prehnite + actinolite ± chlorite ± oxides (prehnite-actinolite facies; Liou, Maruyama, and Cho, 1985; Cho and Liou, 1987). In contrast, a more extreme type of hydrothermal alteration in basaltic rocks consists of replacement of protolith by epidote, prehnite, or Ca-zeolites together with combinations of quartz, chlorite, actinolite, and salite (Balsillie, 1932; Watson, 1953; Harrigan and Maclean, 1976; Marzouki, Kerrich, and Fyfe, 1979; Bird

and others, 1985; Richardson and others, 1987; Schiffman and others, 1987; Rose and Bird, 1987; Schiffman and Smith, 1988; Harper, Bowman, and Kuhns, 1988; Schiffman, Bettison and Smith, 1990). We will refer to this type of alteration as Ca-metasomatism because Ca is added to the protolith, Na and K are removed, and Mg, Fe, and Si may be added or removed depending on local modal variations of the secondary minerals. These types of metasomatic reactions are localized within and near regions of high paleo-permeability such as interpillow regions of basalt flows, miarolitic cavities associated with late stage pegmatites in gabbro plutons, vuggy centers of diabase dikes, and dike parallel fractures and faults.

A diagnostic feature of these metasomatic reaction zones is the absence of Na-rich plagioclase in the final alteration assemblage. Where albite is present it has a resorbed texture and appears to be replaced by CaAl-silicates (Balsillie, 1932; Rose and Bird, 1990). Examples of this paragenesis are illustrated by the microtextures of altered mafic rocks from East Greenland in figure 1. Figure 1A shows an altered diabase dike; the field of view is occupied by prehnite; however, the inclusion-rich outline defines a relict grain of albite. Examination of a suite of samples from the same locality (Rose, ms) reveals a progressive development from albite-bearing diabase to complete replacement of diabase by CaAl-silicates. The mineral textures in these samples show progressive replacement of albite by prehnite. The other principal igneous mineral, clinopyroxene, is often relatively unaltered although the rims may be recrystallized to a more salitic composition. Figure 1B shows replacement of a pegmatitic plagioclase by epidote. Adjacent grains of clinopyroxene are unaltered. The complete replacement of feldspars by hydrous CaAl-silicates is a measure of the extreme Ca / Na exchange that has occurred. This alteration is observed at scales ranging from centimeter scale vesicle alteration to meter wide alteration of dikes.

The metasomatic reactions illustrated in figure 1 involve alteration of a protolith that consisted predominantly of clinopyroxene and plagioclase or clinopyroxene and albite, with minor oxides or olivine. In both cases paragenetic relations suggest that the principal reaction is dissolution of plagioclase or albite and precipitation of CaAl-silicates. The coexisting solutions were undersaturated with feldspar but were either supersaturated or else close to equilibrium with hydrous CaAl-silicates, a situation that would occur if albite or $NaAlSi_3O_8$ in plagioclase were to react with pore fluids that have Na to Ca ratios lower than that required for albite + CaAl-silicate equilibrium. The theoretical models and experiments described below are designed to evaluate the nature of this type of reaction path in terms of elemental mass transfer between hydrothermal solutions, albite, and secondary hydrous CaAl-silicates.

EXPERIMENTAL OBJECTIVE

The experimental objective is to trace the changes in solution chemistry and behavior of solid phases during irreversible dissolution of albite in the presence of prehnite, quartz, and an aqueous solution that contains

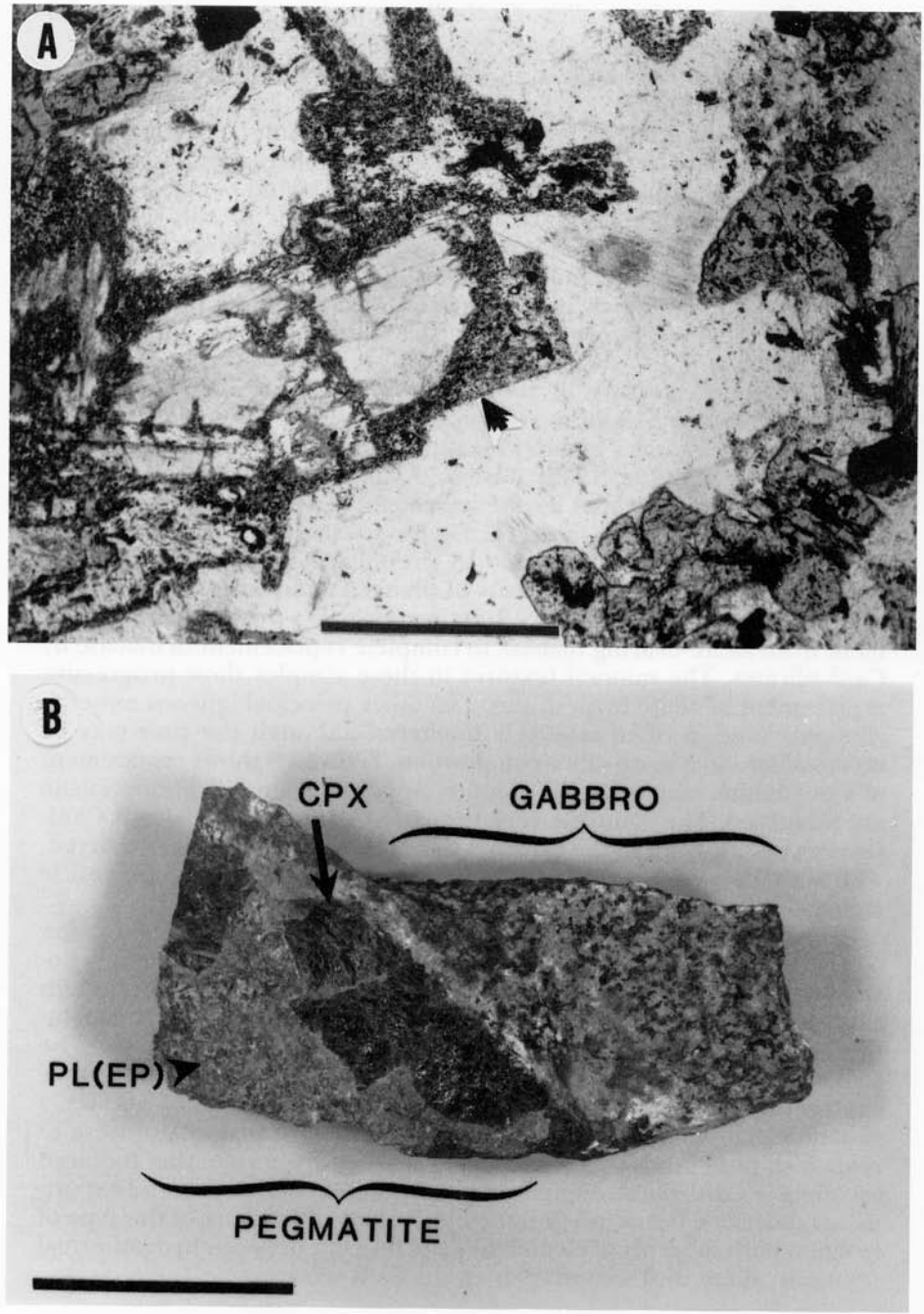

Fig. 1. Textural relations among primary and secondary minerals from hydrothermally altered gabbro and diabase from East Greenland. (A) Prehnite replacing the center of a diabase dike. The arrow points to a blocky outline of an earlier grain of albite that has been replaced by prehnite. Solid inclusions and microporosity in the original albite have been preserved during subsequent replacement by prehnite. The scale bar is 1 mm. (B) Epidote replacement of plagioclase in a late stage pegmatite from the Nordre Aputiteq gabbro. The dark mineral is a primary pegmatitic clinopyroxene that remains virtually unaltered. The scale bar is 5 cm.

known initial concentrations of dissolved $CaCl_2$ and NaCl. The resulting reaction, which is characterized by irreversible hydrolysis of albite and concomitant precipitation of CaAl-silicates and quartz, simulates the replacement of feldspars by Ca-rich phases seen in the natural examples discussed above.

Figure 2 illustrates theoretical phase relations among quartz, albite, paragonite, wollastonite, and CaAl-silicates in the system $CaO–Al_2O_3–SiO_2–H_2O–HCl \pm Na_2O$ at 300°C and 300 bars, as a function of the cation to hydrogen ion activity ratios ($a_{Ca^{2+}}/a^2_{H^+}$), (a_{Na^+}/a_{H^+}), and ($a_{Al^{3+}}/a^3_{H^+}$) and the activity of silica in the coexisting aqueous solution. The activity ratios ($a_{Ca^{2+}}/a^2_{H^+}$) and (a_{Na^+}/a_{H^+}) for the initial solutions in six experiments, labelled AP4 to AP9, are given in figure 2A. Because the solutions initially contained no Al or Si the symbols in figure 2A are projections only, and the solutions are not initially in equilibrium with any of the phases depicted in the diagram. The experiments trace the changes in fluid chemistry during reaction of these initial solutions with albite, quartz, and prehnite along the predicted path shown in figure 2A and C, which is calculated in a later section for a system with an initial composition equivalent to experiments AP4, AP5, AP7, and AP8. The dashed portion of this path is a projection onto the plane of the diagram in figure 2A and C through a third axis that represents log ($a_{Al^{3+}}/a^3_{H^+}$). Although the dashed line crosses the margarite stability field in figure 2A, this is a consequence only of the projection of the diagram, and the fluid is actually undersaturated with margarite.

Experiments were conducted in gold reaction cells and rocking autoclaves (Seyfried, Janecky, and Berndt, 1987). Initial fluid compositions, given in table 1, are between 2.15 to 4.3×10^{-3} m (50–100 ppm) Na and 0.25 to 1.25×10^{-3} m (10–50 ppm) Ca and have a total chloride concentration of approx 5×10^{-3} m. The log ($a_{Ca^{2+}}/a^2_{H^+}$) and log (a_{Na^+}/a_{H^+}) ratios at 300°C and 300 bars were calculated using the EQ3/6 computer code (Wolery, 1983; Wolery and Daveler, in preparation) which determines the distribution of aqueous species at the temperature and pressure of interest. The code was linked to a database generated using thermodynamic data for ions and charged and neutral aqueous complexes from Bourcier, Knauss, and Jackson (1987), Tanger and Helgeson (1988), Shock and Helgeson (1988), Shock, Helgeson, and Sverjensky (1989) and Sverjensky, Hemley and d'Angelo (1991). To obtain local equilibrium with prehnite and quartz during the early stages of the experiments, large amounts of these reactants were included together with relatively small amounts of albite (see table 1).

The relation of the experimental system to theoretical mass transfer calculations is facilitated by evaluating mass balance constraints on the changes in the number of moles of the i'th aqueous species or mineral in the system, n_i, in terms of reaction progress (De Donder and Van Rysselberghe, 1936; Helgeson, 1968; Helgeson and others, 1970):

$$\bar{n}_i = \frac{dn_i}{d\xi}\frac{1}{W_{H_2O}}, \qquad (1)$$

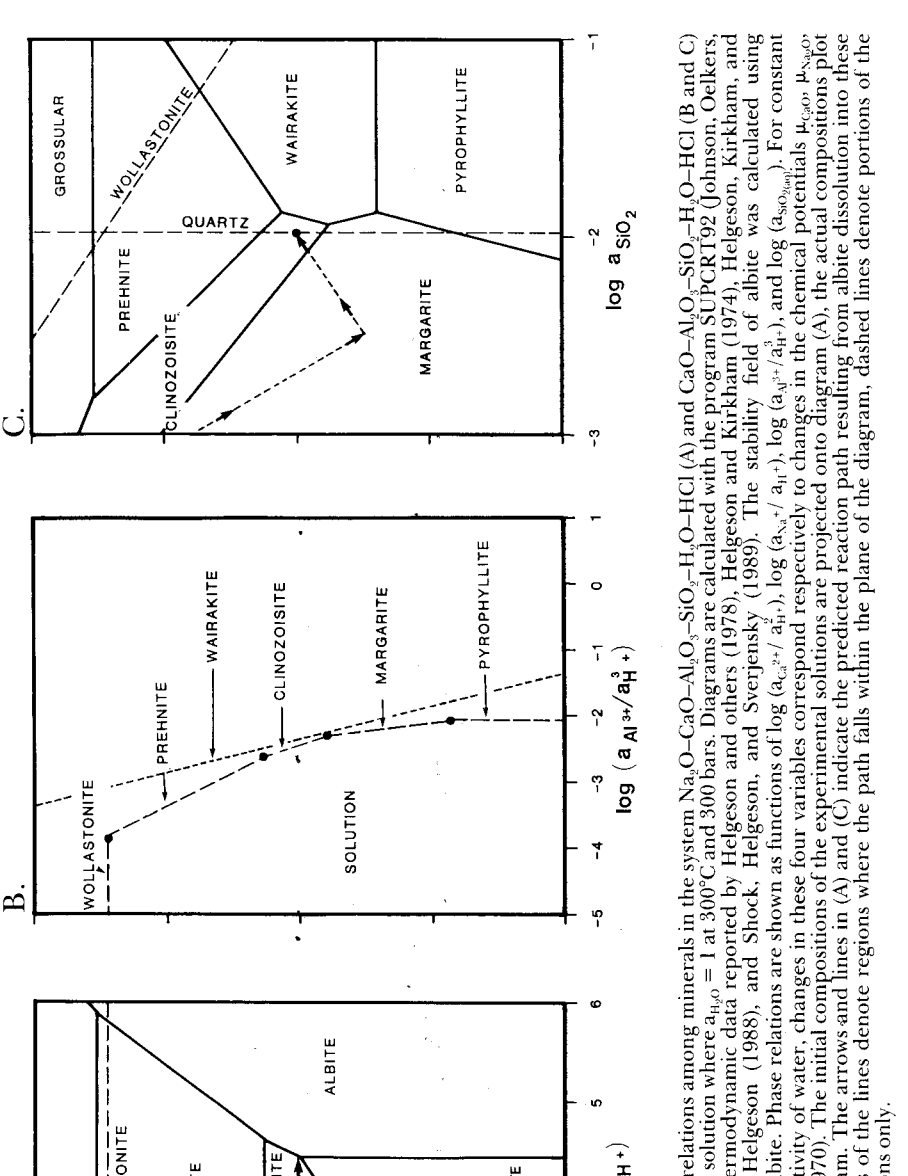

Fig. 2. Theoretical phase relations among minerals in the system Na_2O–CaO–Al_2O_3–SiO_2–H_2O–HCl (A) and CaO–Al_2O_3–SiO_2–H_2O–HCl (B and C) in equilibrium with an aqueous solution where $a_{H_2O} = 1$ at 300°C and 300 bars. Diagrams are calculated with the program SUPCRT92 (Johnson, Oelkers, and Helgeson, 1991) using thermodynamic data reported by Helgeson and others (1978), Helgeson and Kirkham (1974), Helgeson, Kirkham, and Flowers (1981), Tanger and Helgeson (1988), and Shock, Helgeson, and Sverjensky (1989). The stability field of albite was calculated using thermodynamic data for low-albite. Phase relations are shown as functions of log ($a_{Ca^{2+}}/a^2_{H^+}$), log (a_{Na^+}/a_{H^+}), log ($a_{Al^{3+}}/a^3_{H^+}$), and log ($a_{SiO_{2(aq)}}$). For constant pressure, temperature, and activity of water, changes in these four variables correspond respectively to changes in the chemical potentials μ_{CaO}, μ_{Na_2O}, $\mu_{Al_2O_3}$, and $\mu_{SiO_{2(aq)}}$ (Helgeson, 1970). The initial compositions of the experimental solutions are projected onto diagram (A), the actual compositions plot below the surface of the diagram. The arrows and lines in (A) and (C) indicate the predicted reaction path resulting from albite dissolution into these initial solutions. Solid portions of the lines denote regions where the path falls within the plane of the diagram, dashed lines denote portions of the reaction path that are projections only.

TABLE 1

Summary of initial and run conditions

All experiments at 300° C, 300 bars								
	Albite	Prehnite	Epidote	Quartz	$m_{t,Cl}$ x 1000	m_{Na} x 1000	m_{Ca} x 1000	Run Duration (hours)
	mass (grams) *surface area (m^2)*							
AP4	0.1005	0.9749	1.009	4.007	4.88	2.302	1.448	1137
	0.0083	*0.3646*	*0.3309*	*0.25*				
AP5	0.1019	1.0017	-	3.0491	5.00	3.246	0.788	867
	0.0085	*0.3746*	-	*0.191*				
AP6	0.2167	0.9961	-	4.0364	5.021	4.502	0.263	774
	0.018	*0.3725*	-	*0.252*				
AP7	1.0609	0.4841	-	4.0093	5.04	2.315	1.38	527
	0.0881	*0.184*	-	*0.251*				
AP8	3.6317	0.4992	-	5.0987	4.85	2.166	1.339	100
	0.3014	*0.1867*	-	*0.319*				
AP9	0.1019	1.0017	-	3.0491	5.20	4.49	0.263	1183
	0.0085	*0.3746*	-	*0.191*				

where ξ is the reaction progress variable and W_{H_2O} is the mass of water in kilograms. According to this definition $\overline{n}_i$ for aqueous species represents the change in molality. To simplify the notation, $\overline{n}_i$ will be applied to minerals, aqueous species, and total concentrations of aqueous components. Assuming that albite hydrolysis is the only source or sink for Na, then all reactions can be normalized to the dissolution of one mole of albite by specifying:

$$\overline{n}_{albite} = \frac{dn_{albite}}{d\xi}\frac{1}{W_{H_2O}} = -1 = -\overline{n}_{Na}, \tag{2}$$

which requires that

$$dm_{Na} = m_{Na} - m_{Na(initial)} = -dn_{albite}\frac{1}{W_{H_2O}} = d\xi, \tag{3}$$

where m_{Na} is the molality of total sodium in the aqueous solution. Eq 3 indicates that changes in total Na concentration in the fluid are equal to changes in reaction progress. With the exception of AP6 and AP9, the experiments follow a single reaction path depicted in figure 2A and which has an endpoint at albite equilibrium. Experiments AP6 and AP9 have initial compositions that result in convergence with this reaction path at a more advanced stage of reaction. All the experimental results can be referenced to equivalent points in reaction progress by plotting the trends in solution chemistry as a function of Na concentration. Plotting the experimental results against Na concentration, as opposed to time, allows a direct comparison with theoretical mass transfer calculations without reference to specific kinetic models for mineral dissolution

or precipitation. In the following discussion, experimental results are presented first and are then compared to the calculated reaction path. However, during the course of this study the process was iterative, and theoretical calculations were used to optimize initial and run conditions for the experiments.

Reaction progress is related to time via an appropriate kinetic model for albite hydrolysis so that:

$$\overline{n}_{albite} \frac{d\xi}{dt} = R_{albite} S_{albite} = -\overline{n}_{Na} \frac{d\xi}{dt}, \quad (4)$$

where R_{albite} is the rate of albite dissolution in units of mol cm^{-2} s^{-1}, and S_{albite} is the surface area of albite in cm^2. Note that trends in fluid composition or number of moles of minerals dissolved or precipitated that are linear with respect to ξ are non-linear with respect to time because the rate of albite dissolution decreases on approach to albite equilibrium. Inspection of Eq 4 indicates that the overall rate of reaction (that is, $d\xi/dt$) can be varied by changing the initial surface area of albite. The mass of initial albite, and therefore the surface area, was varied by a factor of fifteen in the experiments (see table 1). The purpose was to examine whether this variation in overall reaction rate would affect the reaction path.

EXPERIMENTAL METHODS

Starting minerals.—The compositions, cell edge parameters and surface areas of reactant minerals are summarized in table 2. Albite (from the collection of Dr. R. G. Coleman) from a vein cutting blueschist from Curry County, Oregon, is highly ordered (see footnote to table 2). Prehnite, from a miarolitic cavity in the layered gabbro complex at Nordre Aputitêq, East Greenland, was chosen because of its low Fe^{3+} content (Rose and Bird, 1987). Epidote was used in one experiment; it was purchased from Minerals Unlimited, Ridgecrest, California and originated from Dixie Valley, Nevada. Clear euhedral crystals of quartz were obtained from the Stanford Mineralogical Collection. The minerals were ground to a 100 to 250 micron size fraction and repeatedly washed in acetone and distilled water to remove ultrafine material; the ground material was immersed in concentrated nitric acid and then thoroughly rinsed to remove any Fe contamination during sample preparation. Total mineral mass in each experiment was 6 g or less and the mass of fluid was initially 145 to 160 g. Starting solutions were prepared by dissolving reagent grade Ca and Na chloride in deionized water. The solutions were equilibrated with atmospheric CO_2, and had an initial pH of 5.6 ± 0.2.

Analytical methods.—Up to twelve 6 ml fluid samples were removed from each experiment. The first milliter of fluid was used to flush the exit tube and was then discarded. Of the remaining fluid, one aliquot was used for pH measurement using a microelectrode calibrated with low

TABLE 2

Characterization of starting minerals and run products

	albite*	prehnite**	epidote†	quartz	wairakite‡	wairakite‡	wairakite‡	wairakite‡
SiO_2	69.07	44.01	38.035	101.6	55.34	56.49	55.0	52.98
Al_2O_3	19.10	23.62	27.14	0.28	20.9	21.67	25.2	21.81
TiO_2	-	-	0.16	-	-	-	-	-
Fe_2O_3	0.03	0.283	7.41	-	0.2	0.14	-	0.13
MgO	0.006	-	0.015	-	-	-	-	-
CaO	0.05	26.88	23.56	.03	12.12	12.46	12.41	12.10
MnO	-	-	0.088	-	-	-	-	-
Na_2O	11.69	0.025	-	-	0.07	n.d.	-	-
K_2O	0.02	-	-	-	-	-	-	-
Total	99.97	94.82	96.41	101.91	87.11	92.61	87.11	92.61
				number of atoms per anhydrous oxygen total				
Si	3.01	3.05	3.01	-	4.13	4.11	3.93	4.03
Al	0.98	1.93	2.53	-	1.84	1.86	2.12	1.96
Fe	0.001	0.015	0.44	-	0.01	0.012	-	0.008
Ca	0.002	1.99	1.997	-	0.97	0.97	0.95	0.99
Na	0.989	0.003	0.006	-	-	-	-	-
O	8	11	12.5	-	12	12	12	12
				unit cell parameters				
a	8.145§	4.63	8.894	-	-	-	-	-
b	12.805	5.49	5.581	-	-	-	-	-
c	7.167	18.509	10.173	-	-	-	-	-
α	94.21	-	-	-	-	-	-	-
β	116.598	-	115.444	-	-	-	-	-
γ	87.724	-	-	-	-	-	-	-
Surface area m^2/gram	0.381	0.083	0.215	0.025				

* Wet chemical analysis of low albite from Curry County, Oregon (R.G. Coleman, personal communication).

** Microprobe analysis of prehnite from miarolitic cavity, Nordre Aputitêq, East Greenland.

† Microprobe analysis of epidote from Dixie Valley, Nevada.

‡ Wairakite from experiment AP4.

§ Cell edge parameters together with equation 18 from Helgeson and others (1978; see also, Thompson, Waldbaum, and Hovis, 1974) give a Z ordering parameter of 0.78 which requires 78 percent of the Al to be on the T_1 sites. The Y ordering parameter (Thompson, Waldbaum, and Hovis, 1974) is 0.86 which requires that 86 percent of the T_1 Al to be in the $T_{1,o}$ site.

ionic strength pH buffers; the rest was immediately acidified and diluted for later analysis. Silicon was measured using both the molybdate blue and molybdate yellow methods, Na and Ca were measured by Atomic Absorption (AA) on samples diluted to the range 0 to 1 and 0 to 5 ppm, respectively, and Al was measured on samples diluted to the range 0 to 0.25 ppm using graphite furnace AA. Matrix effects were estimated to be very small in these dilute solutions. Uncertainties for Na and Ca based on 2 standard errors of the calibration curves and dilution errors are

estimated to be approx ±3 percent, with the exception that Ca concentrations of less than 1 ppm have uncertainties of ±10 percent. Reproducibility for the same solutions analyzed on different days was well within these limits. Analytical precision for Al is probably on the order of ±20 percent. A few Al and Fe analyses were also performed using ICP with good agreement with the AA results. Chloride concentrations were measured by titration with $AgNO_3$; uncertainty is estimated to be ±2.5 percent. Chloride analyses before and after experiments indicated that, for the majority of experiments, no change in Cl concentration occurred within this analytical uncertainty. However, in experiment AP5 there was a 17 percent volume increase due to leakage resulting in a dilution of the fluid.

Solid phases were rinsed and examined optically, with scanning electron microscopy (SEM), electron microprobe, and X-ray diffraction (XRD). In general, XRD analysis was unable to resolve the minor amounts of secondary phases in the run products, and thus identification relied on

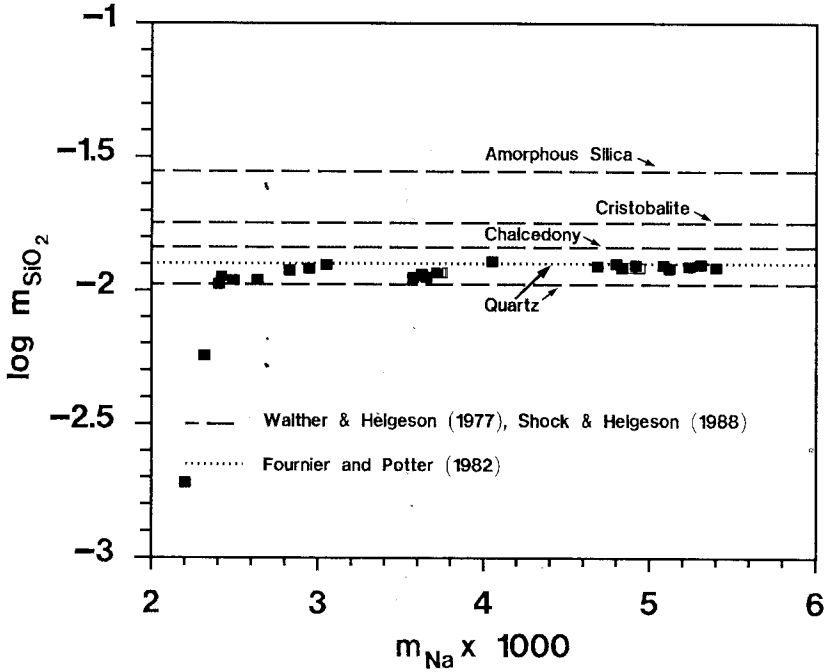

Fig. 3. Summary of analyzed silica concentrations in experiments AP4 to AP9 (square symbols) as a function of Na concentration in millimoles kilogram^{-1}. The solid lines represent solubility of α-quartz, cristobalite, amorphous silica, and chalcedony calculated using data from Walther and Helgeson (1977) and Shock, Helgeson, and Sverjensky (1989), but the dashed line denotes the value of quartz solubility proposed by Fournier and Potter (1982).

morphology, semi-quantitative EDS analysis, and quantitative microprobe analysis on polished mounts.

EXPERIMENTAL RESULTS

Solution chemistry and solid phase behavior.—Changes in solution chemistry during the experiments are summarized in figures 3 to 7. The concentrations of SiO_2(aq) attained a steady state within 50 hrs from the start of each run. These steady state concentrations (fig. 3) have average values for m_{SiO_2} approx 0.05 log units above the predicted solubility of quartz based on data from Walther and Helgeson (1977) and Shock, Helgeson, and Sverjensky (1989) but are close to quartz solubilities reported by Fournier and Potter (1982). All the values are lower than the solubility of other silica polymorphs such as amorphous silica or cristobalite. Horn shaped overgrowths cementing reactant quartz grains in runs AP7 and AP8 are shown in figure 8A. Silicon is the only element detected during EDS analysis of these fine-grained precipitates which are assumed to be microcrystalline quartz. The initial solutions contained no silica, therefore, at an early stage of reaction quartz must have dissolved (that is, $\overline{n}_{quartz}$ was negative). The formation of silica precipitates suggests that after initial silica dissolution $\overline{n}_{quartz}$ was positive.

Sodium and calcium concentrations are shown as a function of time in figure 4. The concentrations of both elements are non-linear with time—the rate of Na increase slows down as the reaction proceeds, and this is matched by a progressively slower rate of decrease in the Ca concentration. The complementary behavior of Na and Ca is illustrated in figure 5. These data indicate an inverse correlation between the total concentrations of Na and Ca in solution which is closely approximated by the expression:

$$\overline{n}_{Ca} = \frac{dm_{Ca}}{dm_{Na}} = \frac{dm_{Ca}}{d\xi} = -0.5. \qquad (5)$$

This relation is independent of the amount of albite initially present in the experiment. Therefore, $\overline{n}_{Ca}$ remains constant, even though the overall release rate of Na to solution has changed significantly between the experiments (compare plots of Na concentration versus time for reactions AP4 and AP8 in fig. 4). Although the data are limited (fig. 5D) it appears that $\overline{n}_{Ca}$ decreases to values less than -0.5 at values of $m_{Na} \times 1000$ greater than 5.

Figure 9 is a compilation of albite dissolution rates from all the experiments, calculated from Na release rates (eq 4) as a function of Na concentration (reaction progress according to eq 3). At early stages of reaction the observed dissolution rates are slightly lower than rates proposed by Helgeson, Murphy, and Aagaard (1984) and Knauss and Wolery (1986) for pH independent albite dissolution. As reaction proceeds the rates decrease by more than an order of magnitude signifying an approach to overall equilibrium with albite.

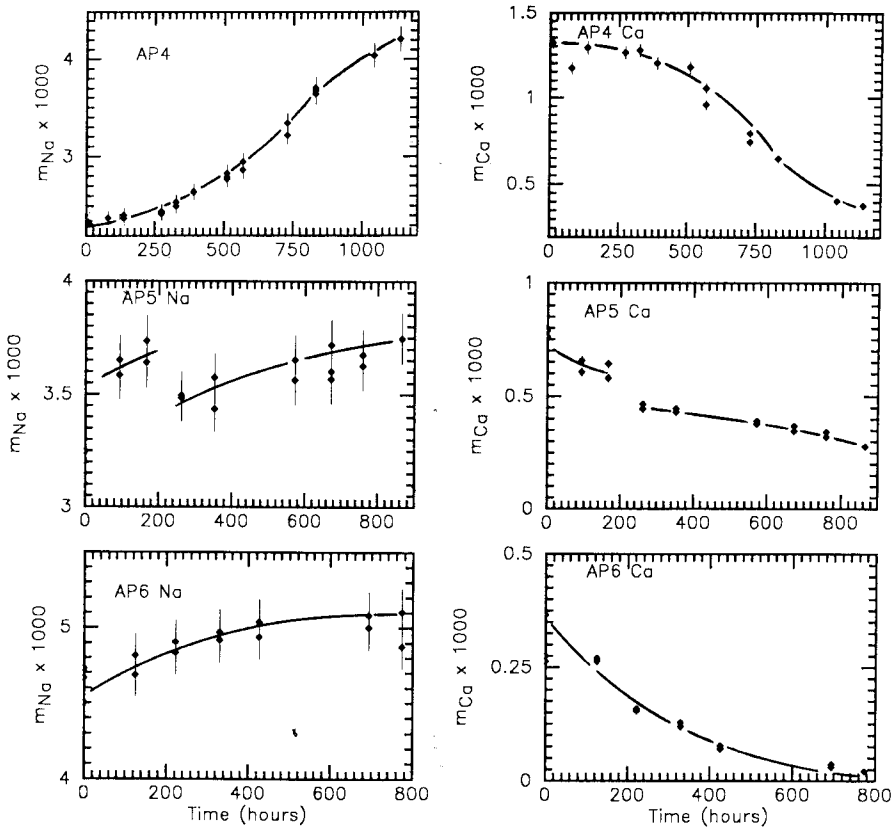

Fig. 4. Measured concentrations of total Na and Ca in experiments AP4 to AP9 expressed as millimoles kilogram^{-1} as a function of time in hours. Error bars represent analytical precision of ±3 percent. Curves are hand-fitted.

The trends in Na and Ca depicted in figures 4 and 5 are consistent with mineralogical and textural observations illustrated in figure 8. In all experiments albite surface textures suggest extensive dissolution in the form of abundant etch pits (see fig. 8C–F). Etch pits are also observed on prehnite surfaces, as shown in figure 8G, indicating that prehnite also dissolved at some stage in the reaction. For the experiment that contained epidote as a starting material (AP4), there was no evidence for reaction of epidote with the aqueous solutions, that is, there were no etch pits or evidence for overgrowths. No major differences in fluid chemistry were seen in subsequent experiments that contained no epidote, suggesting that epidote-fluid reactions had little effect on the observed mass transfer processes in these experiments. In experiments AP4, AP5, AP6,

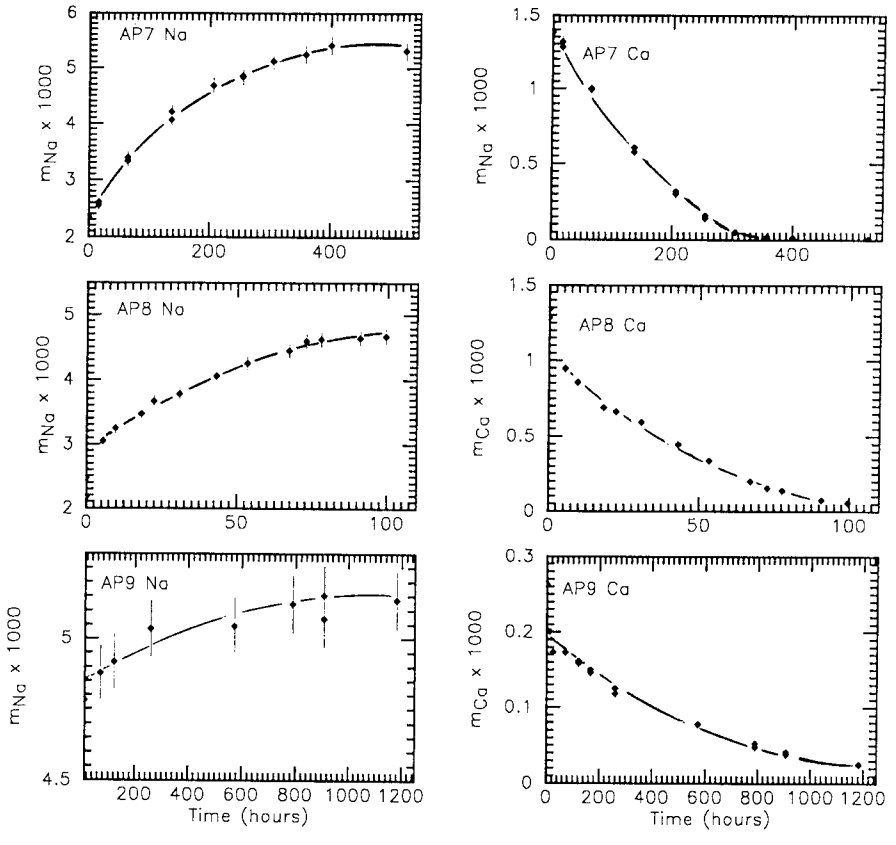

Fig. 4

and AP9 a CaAl-silicate with a euhedral habit grew on all of the reactant grain surfaces. This phase occurs as pseudo-cubic rhombohedral crystals, which frequently show interpenetrative twins (see fig. 8C and 8D), and was identified as wairakite based on microprobe analysis of a polished mount of the run-products given in table 2. Run products from experiments AP7 and AP8, which were characterized by larger amounts of initial albite, contain much finer grained CaAl-silicate grains which have a distinct monoclinic habit and are mainly confined to albite surfaces (see fig. 8E and F). Although these crystals were too fine-grained to be analyzed by microprobe, the habit and relative element concentration based on EDS analysis are indicative of wairakite.

Aluminum concentrations are given in figure 6 as a function of m_{Na}. High values of m_{Al} occur during the early stages of experiment AP4 (fig. 6A), and there is a suggestion of a similar trend in AP8. Aluminum

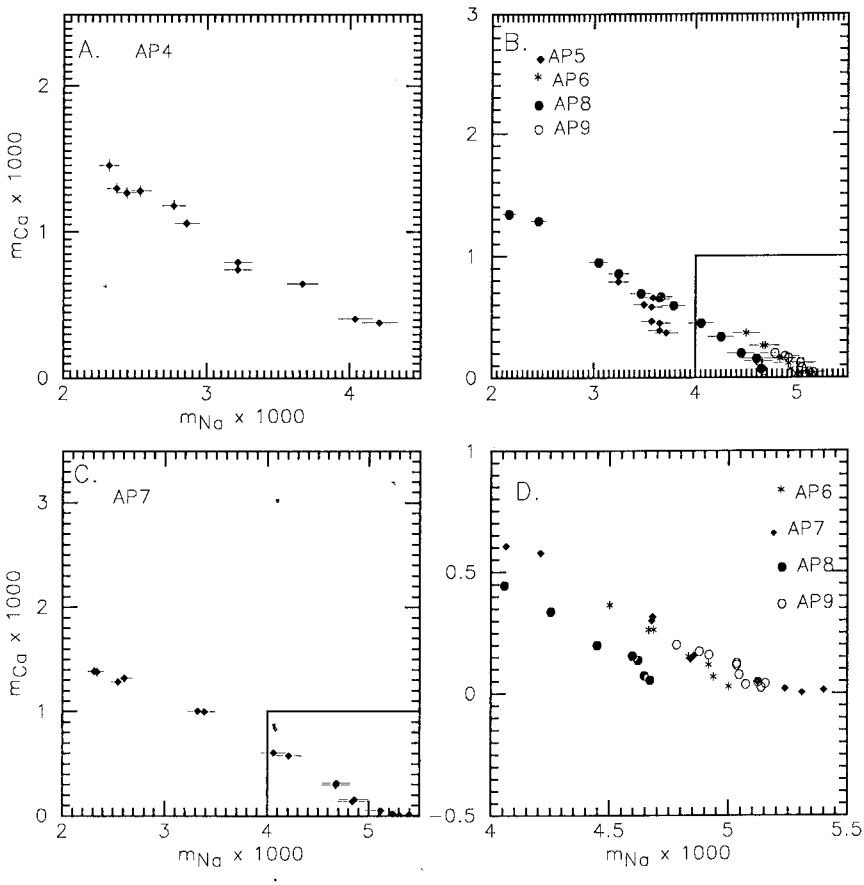

Fig. 5. Measured compositional dependence of Ca and Na during experiments AP4 to AP9 expressed as millimoles kilogram^{-1} of the subscripted element. Diagram (D) represents an expanded view of the regions outlined by boxes in diagrams (B) and (C).

concentrations decrease at intermediate stages of reaction and rise steeply toward the end.

Iron was measured by ICP for experiment AP4 and found to be less than 0.03 ppm (the lower detection limit). Iron was not measured in subsequent experiments to this level of sensitivity, although routine checks using Atomic Absorption indicated Fe levels were always less than the AA detection limit of 0.5 ppm.

Measured pH at 24°C is given in figure 7 as a function of m_{Na}. All values of pH are between 4 and 7.2: the highest values occurred in experiments AP4 and AP9 and were between 5.2 and 7.2. All experiments exhibit a sharp rise in pH at later stages in reaction, and AP4 also

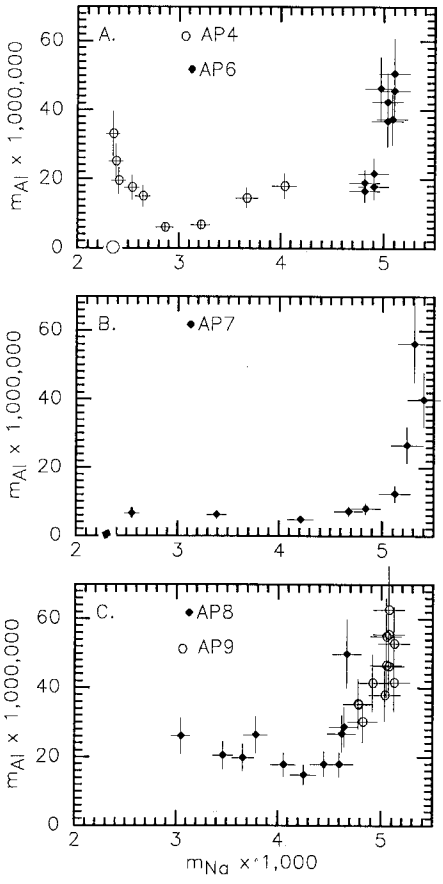

Fig. 6. Measured concentrations of total Al in micromoles kilogram^{-1} as a function of the concentration of total Na in millimoles kilogram^{-1} for five experiments. (A) A summary of experiments AP4 and AP6; (B) AP7; and (C) AP8 and AP9. Error bars are ±20 percent for Al and ±3 percent for Na.

shows a sharp increase at an early stage of reaction. Intermediate stages of reaction are characterized by near constant pH values. Absolute values for pH differed widely between experiments with AP6, AP7, and AP8 giving much lower values than AP4 and AP9. Experiment AP5 showed evidence for leakage of water from the pressure vessel into the gold bag, and it is not considered further. Room temperature speciation calculations using EQ3/6 indicate that combination of the measured pH and solution composition for experiments AP6, AP7, and AP8 results in a positive charge imbalance of 10 percent or more. This could be caused by a 0.5 meq contribution from additional anions other than Cl^- and minor

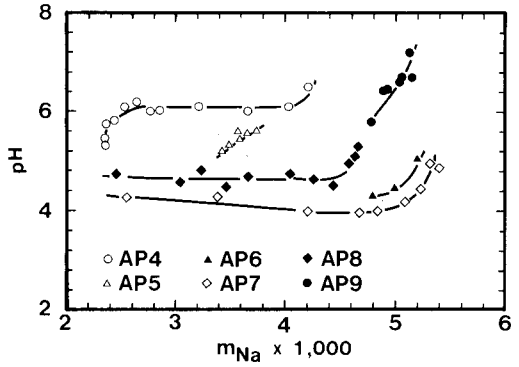

Fig. 7. Measured room temperature pH (24°C) as a function of Na concentration in millimoles kilogram^{-1} in the experimental solutions for experiments AP4 to AP9; solid lines denote trends observed in individual experiments.

$HCO3^-$. In contrast, experiments AP4 and AP9 had charge imbalances that were within analytical error, consequently these solutions are used to calculate in-situ pH below.

Comparison of measured and predicted solution compositions.—Comparison of the measured fluid compositions that occur at the final stages of the experiments with calculated solubilities of the assemblage albite + prehnite + quartz + wairakite are given in table 3 and figure 10. Fluid compositions were calculated using the EQ3/6 computer code. The solid lines in figure 10 are calculated for local equilibrium with albite + prehnite + wairakite at 300°C and 300 bars. The calculations adopt a silica activity of $10^{-1.9}$ consistent with the measured silica concentrations in figure 3. Although these unreversed experiments cannot be used to retrieve solubility data, it is instructive to examine how closely the final solution compositions approach predicted compositions for local equilibrium with albite + CaAl-silicate assemblages.

The symbols in figure 10 represent final fluid compositions from the four experiments (AP6–AP9) which most closely approached steady state values for elements in solution. There is excellent agreement for Na and Al. Dissolved aluminum exists predominantly as the $Al(OH)_4^-$ based on stability constants from Bourcier, Knauss, and Jackson (1987). Measured Ca concentrations are up to 1.5 orders of magnitude higher than calculated values, possibly due to a failure to reach overall equilibrium with albite. Calcium concentration attained steady state only in experiment AP7 but is still a factor of four higher than predicted. This may indicate a failure to account for all possible Ca complexes in solution; in particular, Ca-hydroxide complexes have not been included in the speciation calculations used to define the solid lines in figure 10.

The in-situ pH for experiments AP4 and AP9 was obtained by a two step calculation. Analyzed concentrations of Na, Ca, Al, Cl, together with

the measured pH, were used to calculate room-temperature fluid speciation; bicarbonate concentration was fixed at values consistent with equilibrium with atmospheric CO_2. This process establishes a charge imbalance which is conserved during a subsequent speciation calculation performed at the run temperature. The in-situ pH of the final solution from experiment AP9 is 6.8, 0.4 units below the room temperature value and 0.1 units higher than the calculated value (see table 3).

THEORETICAL ANALYSIS OF THE REACTION PATH AND COMPARISON TO EXPERIMENTAL RESULTS

The experimental results discussed above are characterized by a number of changes in the derivatives of solute concentration and pH with respect to reaction progress. Plotting the fluid chemistry as a function of Na concentration has emphasized certain trends that would be less obvious if time had been used as an independent variable. The reason for this is that albite reacts irreversibly with the fluid throughout the reaction; therefore, the concentration of Na is directly related to reaction progress according to eq 3. The discussion below compares the observed experimental trends in solution chemistry with a theoretical reaction path defined by irreversible dissolution of albite and formation of CaAl-silicates.

The phase relations depicted in figure 2 indicate that prehnite and clinozoisite should buffer the $a_{Ca^{2+}}/a^2_{H^+}$ ratios during the dissolution of albite at values of $a_{SiO_2(aq)}$ controlled by local equilibrium with quartz. However, wairakite formed in all experiments, including AP4 which contained an initial quantity of epidote. Figure 2C shows that the relative stabilities of clinozoisite, prehnite, and wairakite are very sensitive to changes in silica activity; increasing $a_{SiO_2(aq)}$ to values higher than quartz saturation, as observed in the experiments, has the effect of decreasing the width of the clinozoisite stability field that separates wairakite from prehnite. Calculated phase relations for a solution with $\log a_{SiO_2} = -1.9$ (see fig. 3) are given in figure 11. Decreasing the apparent standard molal Gibbs free energy of wairakite by only 141 calories mol^{-1}, compared to the values from Helgeson and others (1978) would eliminate the clinozoisite stability field in figure 11 altogether. In light of the sensitivity of CaAl-silicate phase relations, both to small adjustments in thermodynamic properties and to changes in silica activity, it is not possible to predict if wairakite was in stable or metastable equilibrium with the experimental fluid. Metastable precipitation of wairakite might have occurred if nucleation barriers prevented clinozoisite precipitation. In this case the fluid would evolve along the metastable phase boundary between prehnite and wairakite represented by the dotted line in figure 11. We have made this latter assumption for the purposes of theoretical reaction path calculations discussed below.

Figure 12 summarizes the changes in solution chemistry and mass of reactant and product minerals as a function of ξ during the irreversible hydrolysis of albite, calculated with the computer program EQ3/6 (Wol-

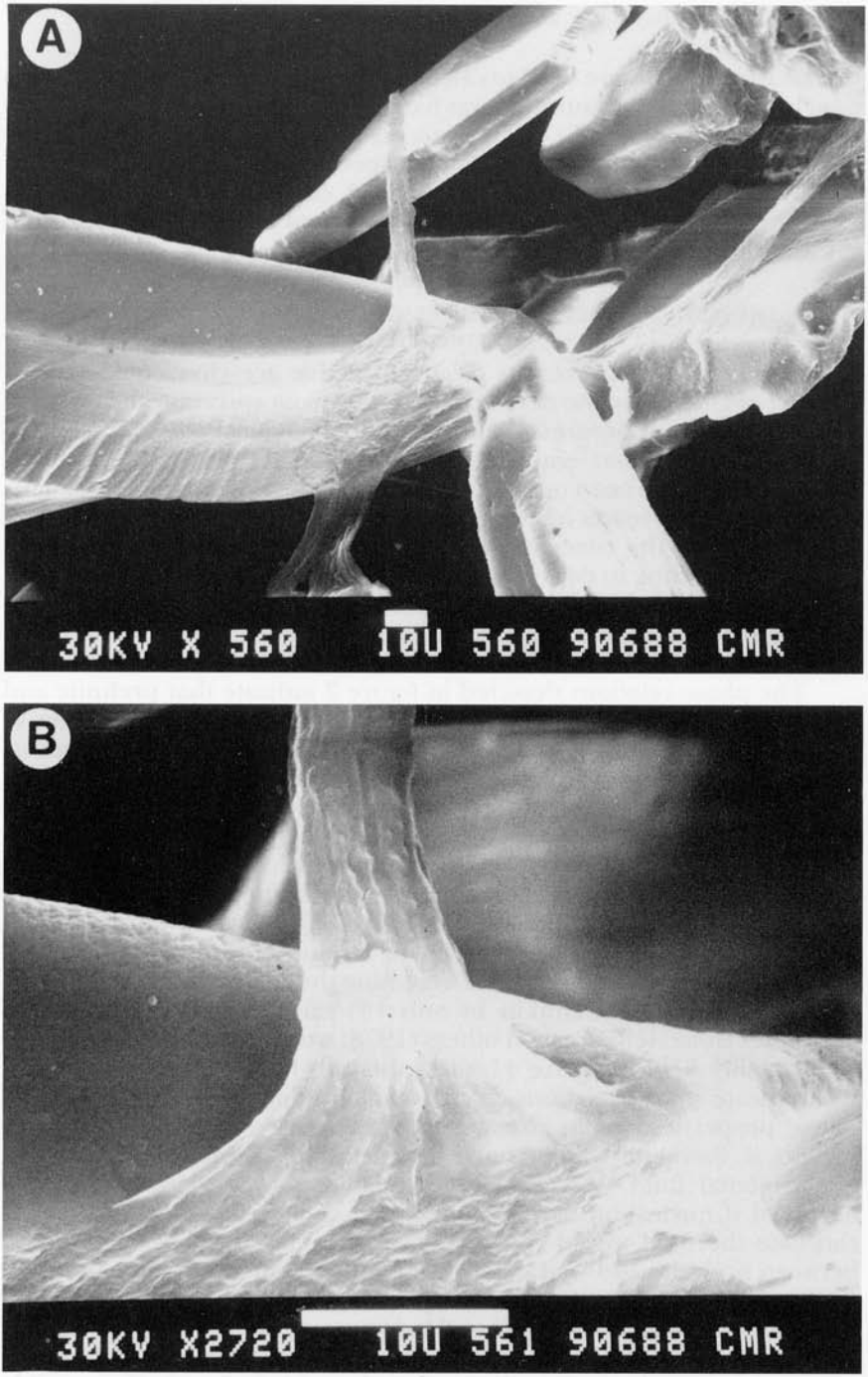

Fig. 8. SEM photographs of secondary minerals formed during experiments AP4 and AP7, scale bars are in microns. (A) and (B) microcrystalline quartz overgrowing quartz grains in experiment AP7.

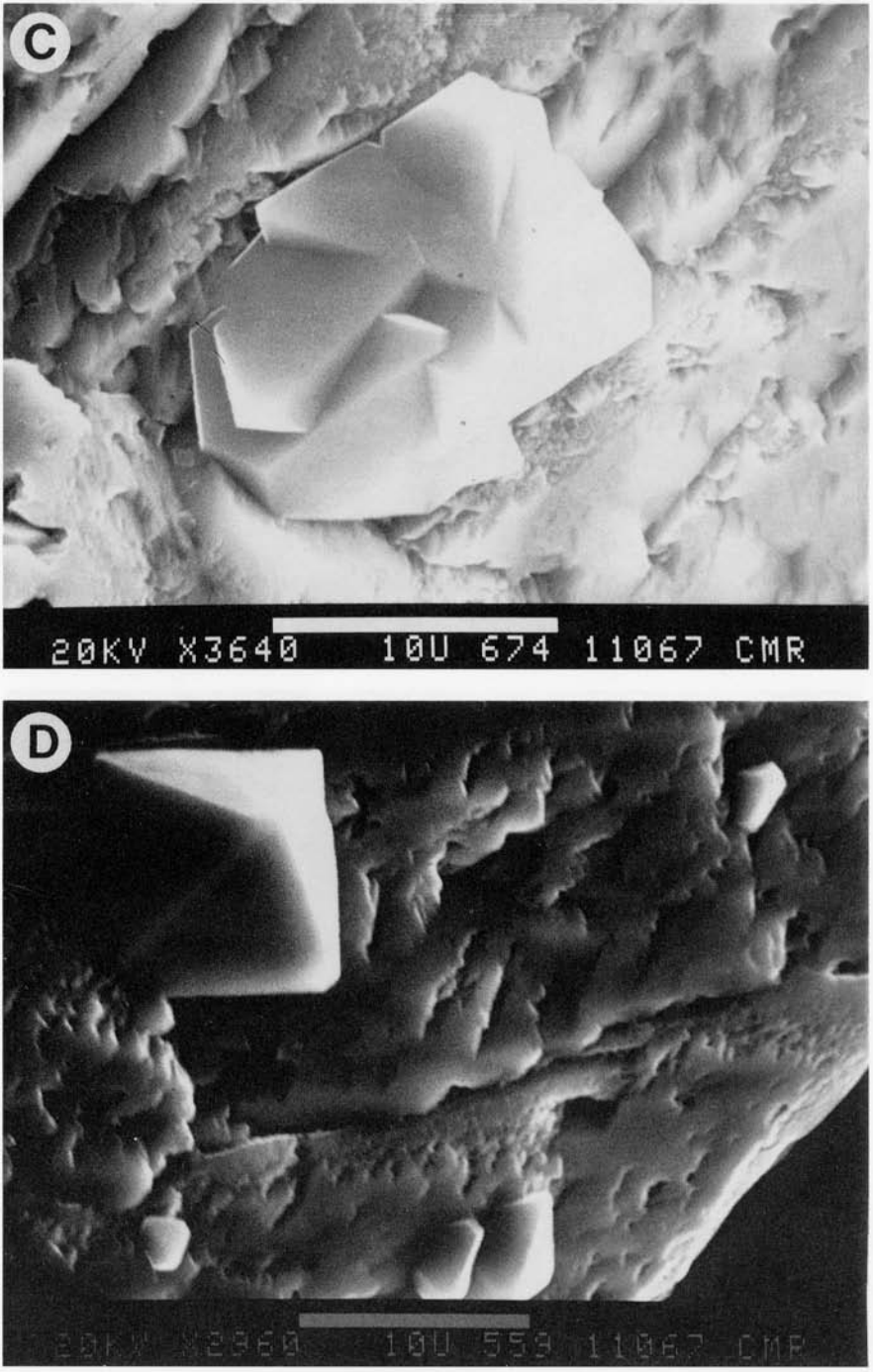

Fig. 8 (continued) (C) and (D) grains of a CaAl-silicate with pseudo-cubic habit and displaying interpenetrating twins growing on an etched albite surface in experiment AP4. This phase is identified as wairakite based on habit and microprobe analysis.

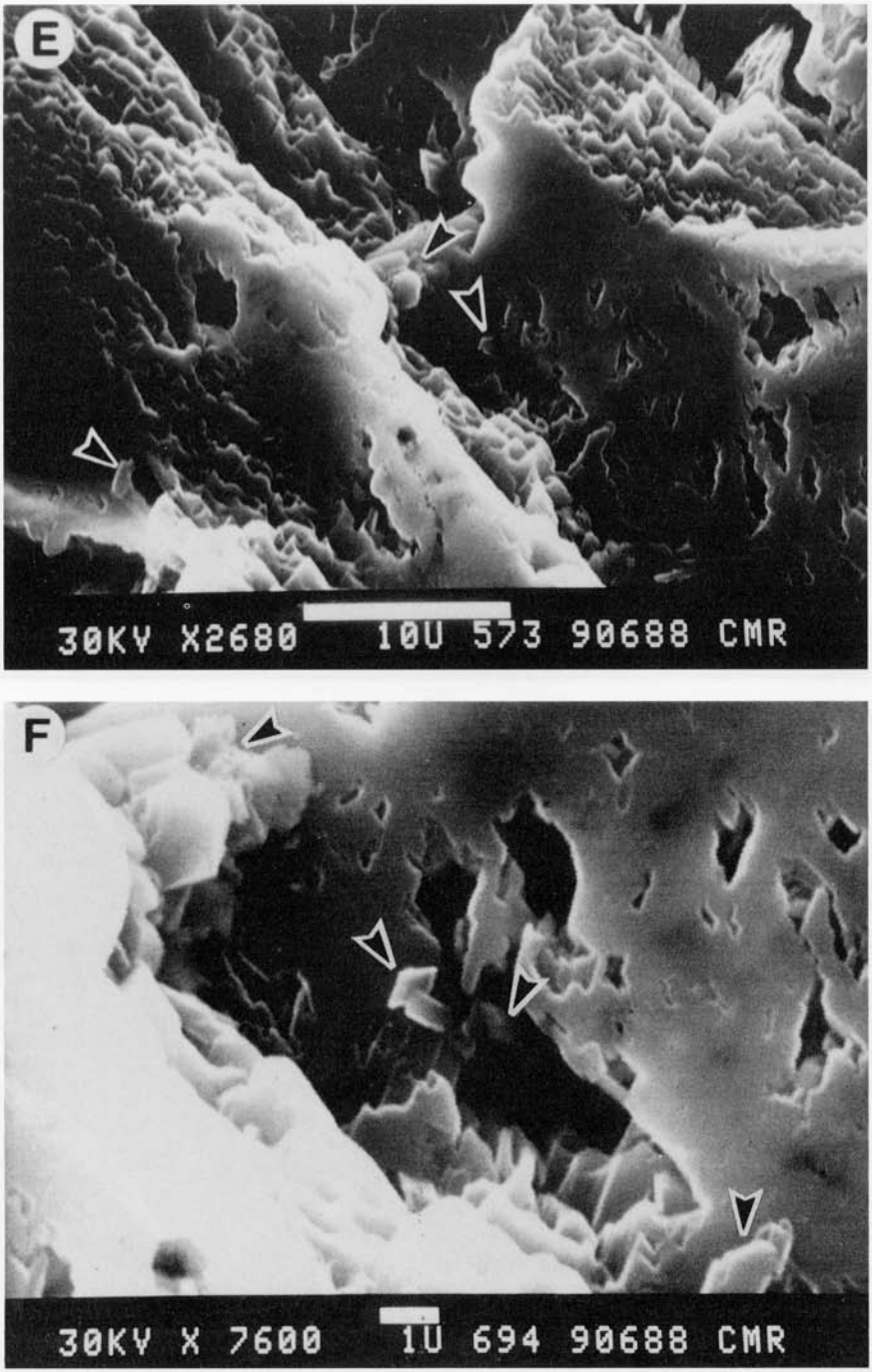

Fig. 8 (continued) (E) and (F) are two different magnifications of secondary CaAl-silicates growing within and near etch pits on albite from experiment AP7. Secondary grains are highlighted with arrows. Crystal habit and semi-quantitative EDS is indicative of wairakite.

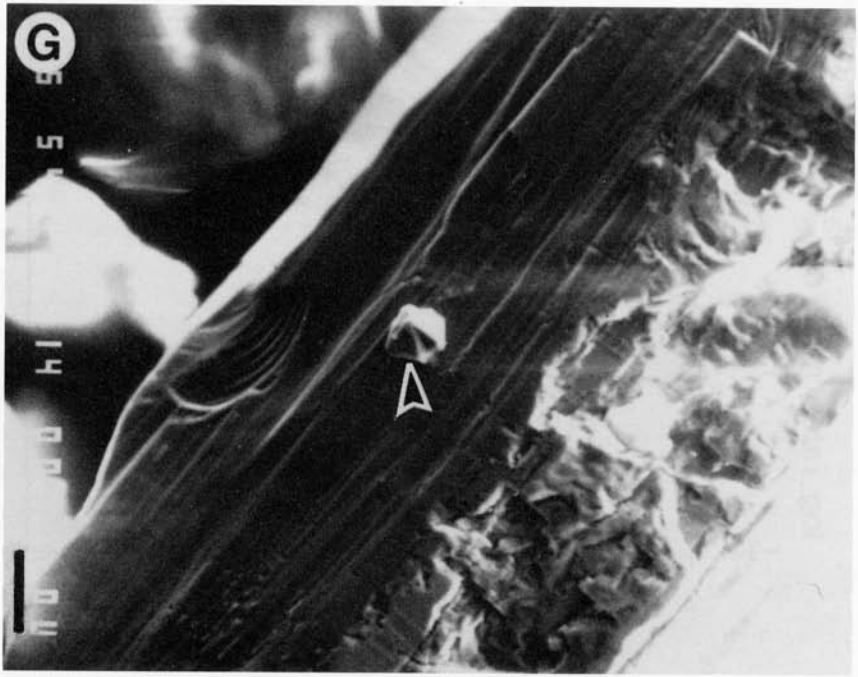

Fig. 8 (continued) (G) Surface of prehnite from experiment AP4 showing growth of wairakite (arrow) and development of etch pits along striations in lower right part of the grain.

ery, 1983; Wolery and Daveler, in preparation). The program calculates the change in concentration of aqueous species, the affinity of product and reactant minerals, and the number of moles of minerals dissolved into or precipitated from solution as a function of reaction progress, where reaction progress is equal to the number of moles of albite dissolved into an initial fluid mass of 1 kg. The starting fluid composition in the computer model corresponds to the initial solution composition in experiment AP4. The relative rates at which the reactants prehnite, albite, and quartz are added to the solution correspond to the relative surface areas of these three minerals in experiment AP4. The vertical stippled lines in figure 12 indicate the point at which albite becomes saturated, at this point there are no further irreversible reactions occurring, and the system has reached overall equilibrium. However, the chemical trends in figure 12 are given to values of ξ beyond this point (achieved by making an arbitrary adjustment to albite stability) in order to illustrate the functional form of equations derived below.

The reaction path can be divided into several regions distinguished by the numbers (i) to (v) in figure 12. When the reaction begins at point (i)

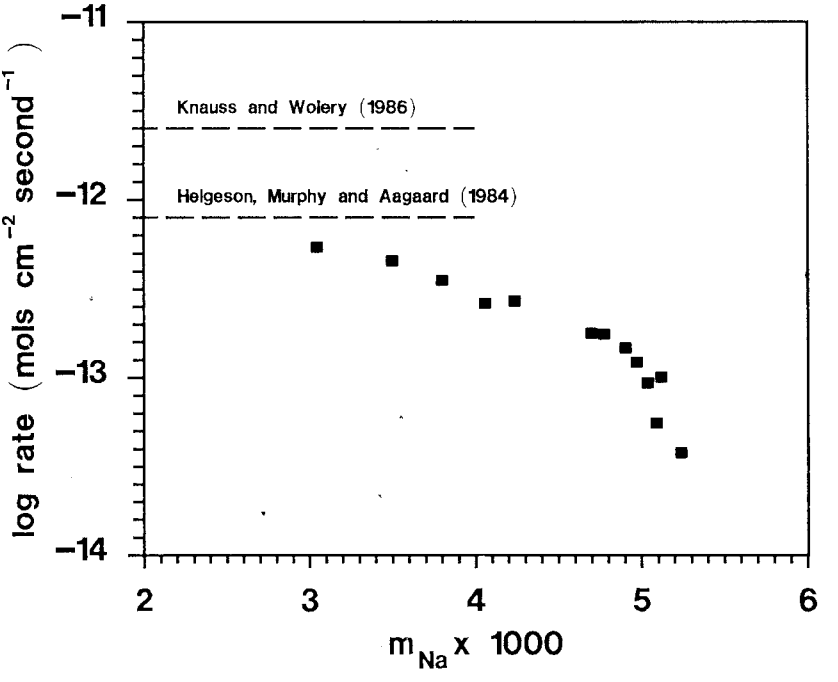

Fig. 9. The computed rates of albite hydrolysis based on total Na release rate to solution as a function of total Na concentration. Dashed lines are the predicted rates of albite hydrolysis at far from equilibrium conditions calculated using pH independent rate laws from Helgeson, Murphy, and Aagaard (1984) and Knauss and Wolery (1986).

there is a sharp increase in pH and Al concentration; at this stage the solution is undersaturated with all phases, and the only heterogeneous reactions are the dissolution of quartz, albite, and prehnite. The dissolution of albite and prehnite are hydrolysis reactions that consume H^+ and release Al, resulting in the large increase in solution pH and Al concentration. The solution is saturated with prehnite at point (ii), and minor precipitation of prehnite at this point prevents further rise in Al concentration and causes the H^+ activity to decrease by 2 orders of magnitude until the solution becomes saturated with wairakite at point (iii). Between point (iii) and (iv) the system is in local equilibrium with prehnite and wairakite but is still undersaturated with quartz and albite. The activity of silica increases due to dissolution of both these phases until point (iv) is reached, and the solution is in local equilibrium with quartz. During this time the pH increases slightly, and Al concentration drops. Between points (iv) and (v) the solution composition is determined by local equilibrium with prehnite, quartz, and wairakite. The only remaining irreversible reaction at this stage is albite hydrolysis. This corresponds to a period of little change in pH and Al concentration, which decreases the

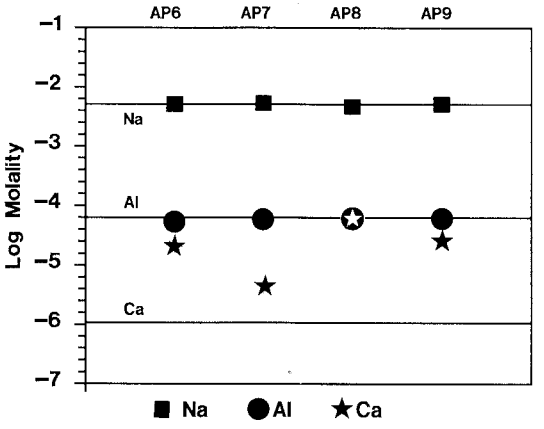

Fig. 10. The concentration of total Na (squares), Al (circles), and Ca (stars) at the end of experiments AP6 to AP9. The solid lines denote calculated solubilities for these elements in equilibrium with albite + prehnite + wairakite at log $a_{SiO_2} = -1.9$. Data for Al hydroxide species used to calculate the theoretical solubilities are from Bourcier, Knauss, and Jackson (1987).

rate of change of albite affinity (fig. 12D). During this stage Ca is removed from solution, and wairakite and quartz precipitate such that $\overline{n}$'s for Ca, wairakite, and quartz are constant. The mass of prehnite is constant so that ($\overline{n}_{prehnite} = 0$). The final stage of reaction begins at $\xi = 0.002$ (point v) and is characterized by a sharp increase in pH and total Al, and a levelling out of the Ca concentration. The increase in Al is directly linked to the increasing pH because Al occurs in solution predominately as negatively charged $Al(OH)_4^-$. Unlike the sharp changes in the derivatives of solute concentration observed earlier in the reaction (points i–iv), this change

TABLE 3

Calculated fluid compositions for local equilibrium with albite + prehnite + quartz + wairakite (EQ3) and observed final fluid compositions in experiments AP6 thru AP9.

	EQ3*	AP6	AP7	AP8	AP9
	log moles kg^{-1} water				
Cl	-2.301	-2.299	-2.297	-2.314	-2.284
Na	-2.287	-2.292	-2.275	-2.331	-2.289
Ca	-5.969	-4.6904	-5.356	-4.259	-4.597
Al	-4.202	-4.295	-4.251	-4.302	-4.255
Si	-1.9	-1.934	-1.917	-1.912	-1.930
pH	6.7	-	-	-	6.8

* Calculated using program EQ3/6 (Wolery, 1983), together with data from following sources: Minerals: Helgeson and others (1978); Ions and Aqueous species: Shock and Helgeson (1988), Shock, Helgeson, and Sverjensky (1989). Hydrolysis constants for Al from Bourcier, Knauss, and Jackson (1987). Dissociation constant for $HCl_{(aq)}$ from Sverjensky, Hemley, and d'Angelo (1991).

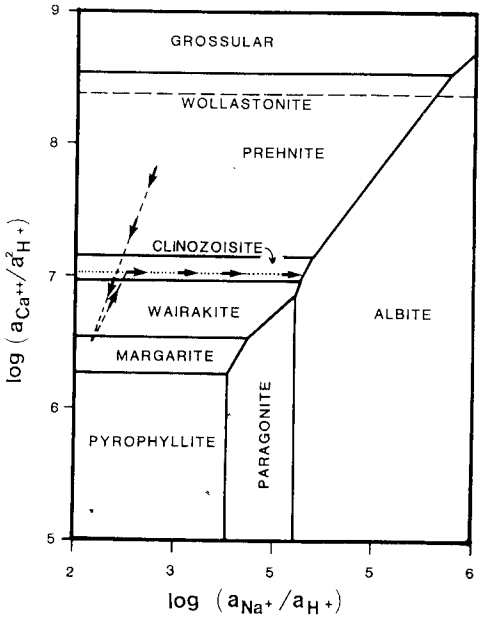

Fig. 11. Phase relations in the system Na_2O–CaO–Al_2O_3–SiO_2–H_2O–HCl at log a_{SiO_2} = −1.9. The diagram is constructed using the thermodynamic data referenced in figure 2. The arrowed line gives the reaction path predicted by the calculations discussed in the text and follows the metastable phase boundary between prehnite and wairakite shown as the dotted line.

does not correspond to saturation with any new mineral phases, instead the exponential increase in pH and the consequent rise in Al solubility are inevitable consequences of the form of mass and charge balance constraints on the system which are discussed below.

Point (v) corresponds to a change in the character of the reaction that has important consequences for Ca-metasomatism. Prior to point (v) one mole of Ca is removed from solution and fixed in secondary Ca phases for every two moles of Na released by albite dissolution. In the context of an open system, these conditions would, over a long term, result in net Ca-enrichment of the rock as CaAl-silicate phases precipitate and replace albite. After point (v) the addition of Na to solution is balanced by the addition of Al, and there is no removal of Ca from the fluid. These contrasting trends are controlled primarily by the charge balance constraints on the system and indicate that the predominant species are Na^+, Ca^{2+}, and $Al(OH)_4^-$. Clearly a very small shift in chemical conditions has resulted in a fundamental change in the nature of the metasomatic reaction associated with albite hydrolysis.

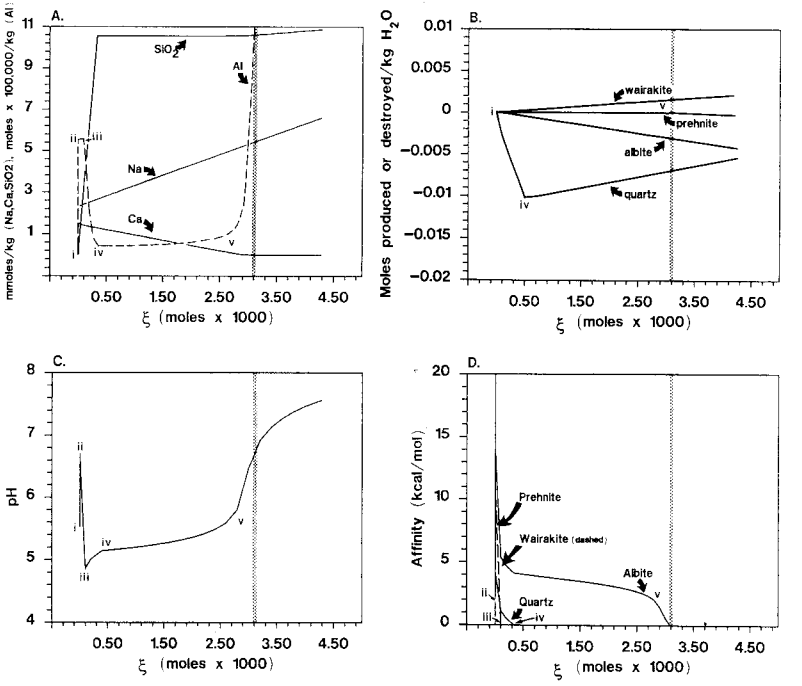

Fig. 12. Trends in chemical variables during irreversible hydrolysis of albite in 1 kg of a dilute aqueous solution with $m_{Cl} = 0.005$ at 300°C and 300 bars, as a function of reaction progress (ξ). The diagrams were calculated using the EQ3/6 computer code (Wolery, 1979, 1983). (A) Total concentrations of elements in solution expressed as 10^{-3} moles of Na, Ca, and Si per kilogram of water and 10^{-5} moles of Al per kilogram of water; (B) number of moles of minerals produced or destroyed; (C) pH, and (D) affinity for the low-albite, prehnite, and quartz. Positive values for affinity denote undersaturation of the aqueous solution with respect to the mineral. For comparison of diagram (B) to the experimental system described in this study, the number of moles of minerals produced or destroyed as shown in the diagram should be normalized to account for the actual mass of solution in the experiment which is less than 1 kg. Activity coefficients for charged aqueous species are calculated using an extended Debye–Hückel equation (the B dot equation of Helgeson, 1969). The initial solution closely approximates the initial solution composition for experiments AP4, AP5, AP7, and AP8 and is 5×10^{-3} m total Cl, 2.1×10^{-3} m (45 ppm) Na, and 1.5×10^{-3} m (56 ppm) Ca. The vertical dashed lines in (A), (B), and (C) denote saturation with albite and saturation is the real endpoint of the reaction; the metastable continuation of the reaction beyond this point is shown to illustrate the trends discussed in the text. Points marked (i) through (v) represent: (i) start, (ii) saturation with prehnite, (iii) saturation with wairakite, (iv) saturation with quartz, (v) beginning of pH inflexion.

Many of the features of the reaction discussed above and in figure 12 are readily observable in the experiments. First, quartz was initially undersaturated, but silica concentration rose during reactant mineral dissolution, levelling off at a value slightly higher than quartz saturation, and silica overgrowths were observed in the run products. These observations are consistent with $\overline{n}_{quartz}$ changing from negative to positive, be-

cause after quartz saturation was reached, continued addition of silica to solution from albite dissolution was not completely balanced by silica removal due to wairakite precipitation. The slight supersaturation of silica concentration with respect to quartz and its precipitation as a microcrystalline form (fig. 8A and B) reflects the ability for quartz nucleation and precipitation to keep pace with the continued addition of silica to solution from albite dissolution.

Measured Al concentration and pH in experiments AP4, AP6, and AP9 are compared to the theoretical trends in figure 13. The initial sharp increase in pH between points (i) and (ii) was not observed in any of the experiments. However, this occurs at extremely small values of ξ, and it is possible that these early variations are obscured by the time taken to heat the pressure vessel to temperature (about 8 hrs). Alternatively, the assumptions adopted in the reaction path model, such as stoichiometric dissolution of the reactant minerals with thermodynamic properties representative of the bulk mineral structure, may be invalid at these small extents of reaction. Because these early stages of reaction involve very little mass transfer, transient non-stoichiometric dissolution, or surface adsorption or desorption reactions may be involved. The maxima in Al concentration was however seen in AP4 and AP8, suggesting that the uptake of Al was partly controlled by the nucleation and precipitation rates of wairakite. The trend of increasing solution pH between points (iii) and (iv) is also observable in the results from AP4.

The closest correlations between experimental and theoretical results are seen between points (iv) and (v), where the observed pH and Al concentrations are fairly constant, and the change in solution composition is dominated by addition of Na and removal of Ca. The molal ratio of Na added to solution against Ca removed by secondary phase precipitation is constant throughout most of the experiments (fig. 5) and was not modified even when the amount of albite surface area was increased by a factor of 15. This suggests that the overall growth rate of secondary Ca-bearing phases increased in experiments with larger overall reaction rates (as defined by eq 4) so that trends in solution chemistry exhibit little variation. Examination of the run products demonstrates that these differing rates of Ca-uptake are related to different habits of secondary CaAl-silicates, specifically increased overall rate of reaction according to eq 4 increased the number but decreased the size of wairakite grains. Wairakite may have become more supersaturated in those experiments that had larger amounts of albite, resulting in an increased wairakite nucleation/growth rate. As the reaction proceeds the trends in solution chemistry undergo a large, but continuous change, characterized by increased $\overline{n}_{Al}$ and $\overline{n}_{H^+}$ and decreased $\overline{n}_{Ca}$; these changes are clearly seen in the experimental results. The trends in pH and Al are observed in all experiments while the decrease in $\overline{n}_{Ca}$ is observed in AP7 and to a lesser extent in AP9.

At values of ξ beyond point (iv) the system is in local equilibrium with wairakite, prehnite, and quartz, and the only irreversible reaction in the

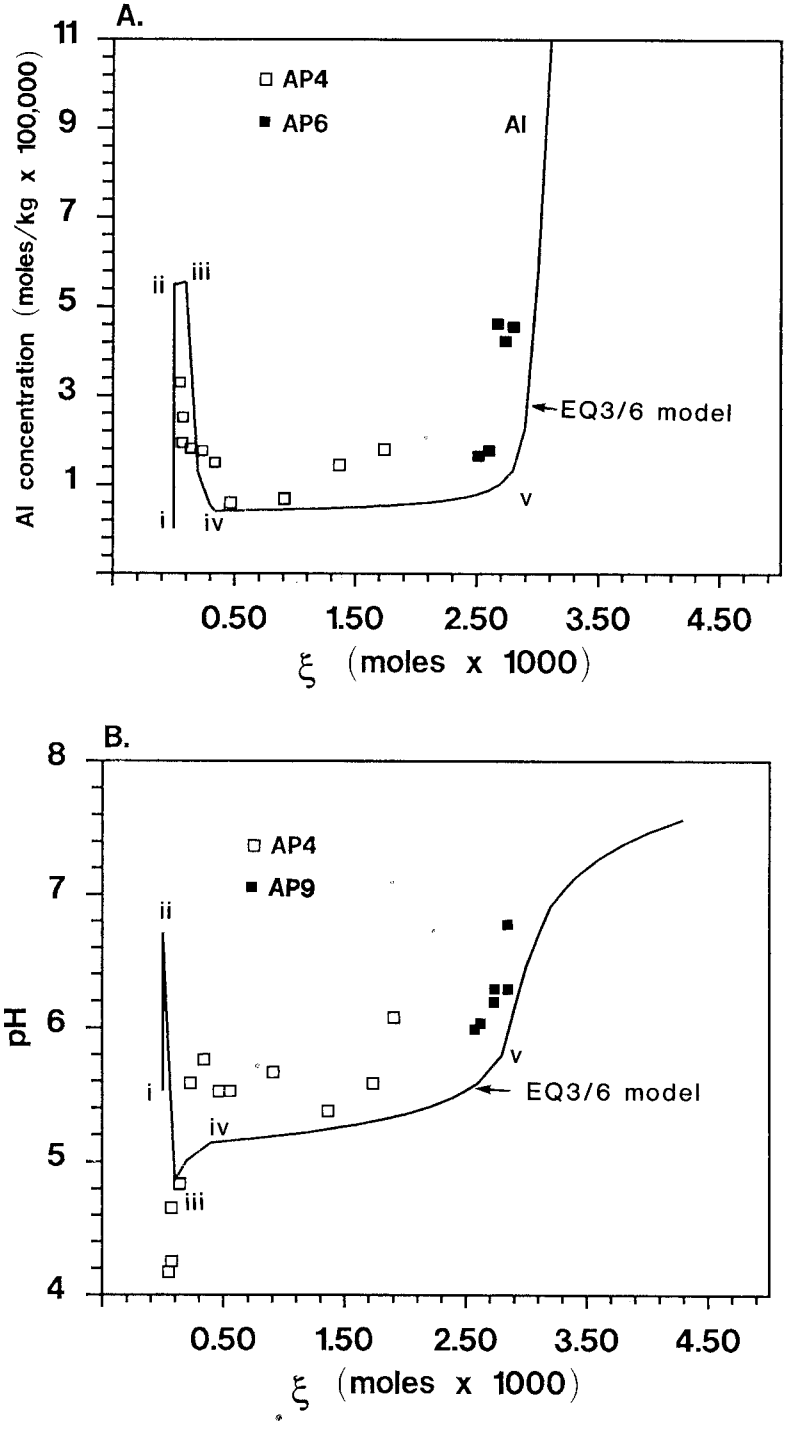

Fig. 13. Superimposition of experimental data from runs AP4, AP6, and AP9 onto (A) calculated trend for Al and (B) pH. The experimental points are expressed in terms of ξ by subtracting the initial Na molality in experiment AP4 from the actual Na molality. pH is recalculated for the in-situ temperature as discussed in the text.

system is albite hydrolysis. For these conditions it is possible to derive a set of equations that describe the form of the curves in figure 12. These are derived by progressive simplification of the grand matrix that defines the mass balance constraints on the system (Helgeson and others, 1970; Helgeson, 1979). The purpose of these equations is to evaluate the local equilibrium constraints on differential changes ($\bar{n}$) for the dominant aqueous species which are Cl^-, $Al(OH)_4^-$, Na^+, Ca^{2+}, H^+, OH^-, H_2O, and $SiO_{2(aq)}$, and the secondary phases wairakite, prehnite, and quartz, during the irreversible hydrolysis of albite. These calculations assume that activity coefficients are constant and close to unity in these dilute solutions. The resulting matrix is given in table 4. The first seven rows represent mass balance equations for the elements Cl, Al, Ca, Na, Si, H, and O and have the form:

$$\sum_{i}^{I} \hat{n}_{\epsilon,i}\bar{n}_i = -\hat{n}_{\epsilon,albite}\bar{n}_{albite}, \tag{5}$$

where $\hat{n}_{\epsilon,i}$ is the stoichiometric coefficient for the ϵth element in the ith aqueous species or mineral. The last four rows represent the law of mass action for the dissociation of H_2O, the solubility of quartz, and the computed hydrolysis of prehnite and wairakite as required by local equilibrium of these minerals with the aqueous solution. These equations have the general form of:

$$\frac{d \ln K_r}{d\xi} = 0 = \sum_{i}^{I} \hat{n}_{i,r} \frac{d \ln m_i}{d\xi} = \sum_{i}^{I} \frac{\hat{n}_{i,r}\bar{n}_i}{m_i}, \tag{6}$$

The matrix presented in table 4 can be progressively simplified on account of experimental and theoretical constraints discussed below. Closed system dissolution of albite in local equilibrium with quartz leads to the following identities:

$$\bar{n}_{Na^+} = -\bar{n}_{albite} = 1.0, \tag{7}$$

$$\bar{n}_{Cl^-} = 0, \tag{8}$$

and

$$\bar{n}_{SiO_{2(aq)}} = 0. \tag{9}$$

Eq 7 arises because albite is the only Na-bearing phase participating in the reaction. Eqs 8 and 9 follow from the fact that chloride is neither produced nor consumed by reactions occurring during the experiment and because the concentration of silica is constrained by local equilibrium with quartz.

Local equilibrium among prehnite, wairakite, quartz, and an aqueous solution in the experiment can be expressed by the reactions:

$$\underset{prehnite}{Ca_2Al_2Si_3O_{10}(OH)_2} + 2H^+ + \underset{quartz}{SiO_2} = \underset{wairakite}{CaAl_2Si_4O_{12}\cdot 2H_2O} + Ca^{2+} \tag{10}$$

TABLE 4

Grand matrix for irreversible albite hydrolysis in local equilibrium with prehnite, wairakite, and quartz.

	Cl^-	$Al(OH)_4^-$	Ca^{2+}	Na^+	SiO_2	H^+	OH^-	H_2O	qtz	pr	wrk				
Cl	0	0	0	0	0	0	0	0	0	0	0		$\bar{n}_{Cl^-}$		0
Al	0	1	0	0	0	0	0	0	0	2	2		$\bar{n}_{Al(OH)_4^-}$		1
Ca	0	0	1	0	0	0	0	0	0	2	1		$\bar{n}_{Ca^{2+}}$		0
Na	0	0	0	1	0	0	0	0	0	0	0		$\bar{n}_{Na^+}$		1
Si	0	0	0	0	1	0	0	0	1	3	4		$\bar{n}_{SiO_2}$		3
H	0	0	0	0	0	1	1	2	0	2	4		$\bar{n}_{H^+}$		0
O	0	0	0	0	2	0	1	1	2	12	14	X	$\bar{n}_{OH^-}$	=	8
H_2O	0	0	0	0	0	$\frac{1}{m_{H^+}}$	$\frac{1}{m_{OH^-}}$	0	0	0	0		$\bar{n}_{H_2O}$		0
quartz	0	0	0	0	$\frac{1}{m_{SiO_2}}$	0	0	0	0	0	0		$\bar{n}_{qtz}$		0
prehnite	0	$\frac{2}{m_{Al(OH)_4^-}}$	$\frac{2}{m_{Ca^{2+}}}$	0	$\frac{3}{m_{SiO_2}}$	$\frac{-2}{m_{H^+}}$	0	0	0	0	0		$\bar{n}_{pr}$		0
wairakite	0	$\frac{2}{m_{Al(OH)_4^-}}$	$\frac{1}{m_{Ca^{2+}}}$	0	$\frac{4}{m_{SiO_2}}$	0	0	0	0	0	0		$\bar{n}_{wrk}$		0

and

$$CaAl_2Si_4O_{12}\cdot 2H_2O + 1.0H_2O = 0.5Ca_2Al_2Si_3O_{10}(OH)_2 + 2.5SiO_2$$
wairakite *prehnite* *quartz*

$$+ Al(OH)_4^- + H^+. \quad (11)$$

For which the mass action equations require that

$$K_{10} = \frac{m_{Ca^{2+}}}{m_{H^+}^2}, \quad (12)$$

and

$$K_{11} = m_{Al(OH)_4^-} m_{H^+}. \quad (13)$$

Differentiating eqs 12 and 13 with respect to ξ requires:

$$\bar{n}_{Ca^{2+}} = 2K_{10} m_{H^+} \bar{n}_{H^+}, \quad (14)$$

and

$$\bar{n}_{Al(OH)_4^-} = -K_{11} m_{H^+}^{-2} \bar{n}_{H^+}. \quad (15)$$

Similarly the law of mass action for H_2O dissociation can be differentiated to give,

$$\bar{n}_{OH^-} = -K_w m_{H^+}^{-2} \bar{n}_{H^+}, \quad (16)$$

where K_w is the dissociation constant for water.

TABLE 5

Reduced form of the grand matrix in Table 4.

	H^+	H_2O	quartz	prehnite	wairakite				
Al	$-K_{11}m^{-2}_{H^+}$	0	0	2	2		$\bar{n}_{H^+}$		1
Ca	$2K_{10}m_{H^+}$	0	0	2	1		$\bar{n}_{H_2O}$		0
Si	0	0	1	3	4	X	$\bar{n}_{qtz}$	=	3
H	$1-\frac{K_w}{m^2_{H^+}}$	2	0	2	4		$\bar{n}_{pr}$		0
O	$-\frac{K_w}{m^2_{H^+}}$	1	2	12	14		$\bar{n}_{wrk}$		8

The experimental constraints of local equilibrium and mass transfer expressed by eqs 7 through 16 reduce the grand matrix in table 4 to the 5 by 5 matrix shown in table 5. For example, the row representing the law of mass action for prehnite is eliminated as follows:

$$\frac{4K_{10}m_{H^+}\bar{n}_{H^+}}{K_{10}m^2_{H^+}} - \frac{2K_{11}m^{-2}_{H^+}\bar{n}_{H^+}}{K_{11}m^{-1}_{H^+}} - \frac{2\bar{n}_{H^+}}{m_{H^+}} = 0. \tag{17}$$

A further constraint on the system arises from the electroneutrality condition expressed in derivative form as:

$$2\bar{n}_{Ca^{2+}} + \bar{n}_{H^+} - \bar{n}_{Al(OH)_4^-} - \bar{n}_{OH^-} = -\bar{n}_{Na^+}. \tag{18}$$

Substituting eqs 14 to 16 into eq 18 and rearranging gives

$$\bar{n}_{H^+} = -(4K_{10}m_{H^+} + K_{11}m^{-2}_{H^+} + K_w m^{-2}_{H^+} + 1)^{-1}. \tag{19}$$

Iterative solution to eq 19 indicates that the parenthetical term on the right side passes through a minimum and subsequently increases. This minimum corresponds to the inflexion point in the pH curve at point (v) in figure 12C.

During stages of the reaction between points (iv) and (v) in figure 12 the first parenthetical term in eq 19 predominates such that:

$$2K_{10}m_{H^+}\bar{n}_{H^+} = \bar{n}_{Ca^{2+}} \approx -0.5. \tag{20}$$

The first two rows of the matrix in table 5 thus reduce to:

$$0 + 2\bar{n}_{prehnite} + 2\bar{n}_{wairakite} = 1, \tag{21}$$

and

$$-0.5 + 2\bar{n}_{prehnite} + \bar{n}_{wairakite} = 0, \tag{22}$$

so that:

$$\bar{n}_{wairakite} = 0.5, \tag{23}$$

and

$$\bar{n}_{prehnite} = 0. \tag{24}$$

Substituting these values into table 5 requires that $\bar{n}_{quartz} \sim 1$ and that $\bar{n}_{H_2O} \sim -1$. Note that as the reaction proceeds $\bar{n}_{Ca^{2+}}$ increases to values greater than -0.5, and $\bar{n}_{Al(OH)_4^-}$ becomes an increasingly large positive number.

These simplifying assumptions clarify the relation between trends in solution chemistry and mineral-fluid reactions under local equilibrium constraints that exist over a large extent of the experimental reaction. Unlike the discontinuities that occur at early stages of reaction and that correspond to saturation of the fluid with respect to intermediate secondary phases, these latter non-linear trends are continuous and are demonstrable consequences of the mass and charge balance constraints on the system. The stages of reaction described by eqs 5 through 24 correspond to local equilibrium with CaAl-silicates but irreversible dissolution of albite. Based on the paragenetic observations described earlier, this may resemble the situation during Ca-metasomatism whereby albite is replaced by CaAl-silicates.

The overall volume change of the solid phases during the metasomatic replacement of albite in the experimental system can be approximated by summing the products of $\bar{n}$ for the minerals and their molar volumes. Note that between points (iv) and (v) in figure 12 the values of $\bar{n}$ for minerals are approximately constant, and the total volume change can therefore be expressed as:

$$\Delta V_{solids} = 0.5V^{o}_{wairakite} + V^{o}_{quartz} - V^{o}_{albite}, \quad (25)$$

where V^{o} is the molar volume of the subscripted mineral in $cm^3\ mol^{-1}$. Adopting molar volumes reported by Helgeson and others (1978) for low-albite and quartz and Donnay and Ondik (1973) for wairakite indicates that ΔV_{solids} calculated from eq 25 is positive with a value of 18.2 $cm^3\ mol^{-1}$ per mole of albite dissolved. Because the molar volume of low-albite is 100.07 $cm^3\ g^{-1}$ this represents a 18.2 percent volume increase in solid phases for each mole of albite dissolved. In contrast, ΔV_{solids} for an equivalent reaction in which clinozoisite nucleates in place of wairakite is negative and corresponds to a 9.3 percent reduction in volume.

DISCUSSION

Calcium metasomatism in basaltic systems.—The good correlation between theoretical and experimental approaches demonstrates the applicability of reaction path modeling for predicting the course of mineral-fluid reactions in high temperature systems. However, to apply these observations to natural systems, it is necessary to extend the closed system isothermal and isobaric reaction to open system fluid flow in the presence of temperature and pressure gradients. A limitation of the closed system approach is that the initial disequilibrium between the fluid and the reactant minerals was artificially induced by selecting starting solutions that met the criteria of undersaturation with albite, prehnite, and quartz. The following discussion illustrates how, in natural systems,

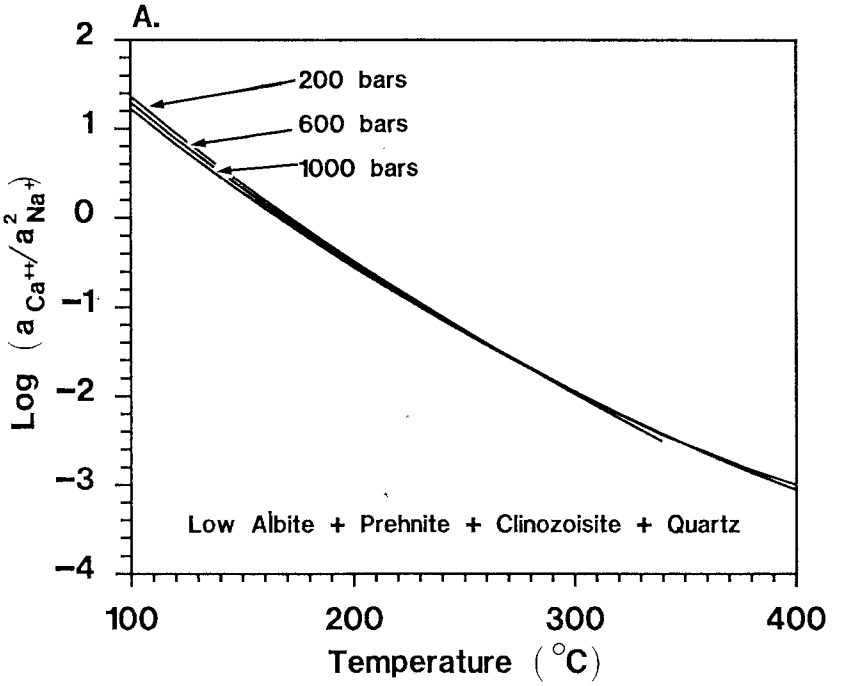
A.
2
1
0
−1
−2
−3
−4
Log ($a_{Ca^{++}}/a^2_{Na^+}$)
200 bars
600 bars
1000 bars
Low Albite + Prehnite + Clinozoisite + Quartz
100
200
300
400
Temperature (°C)

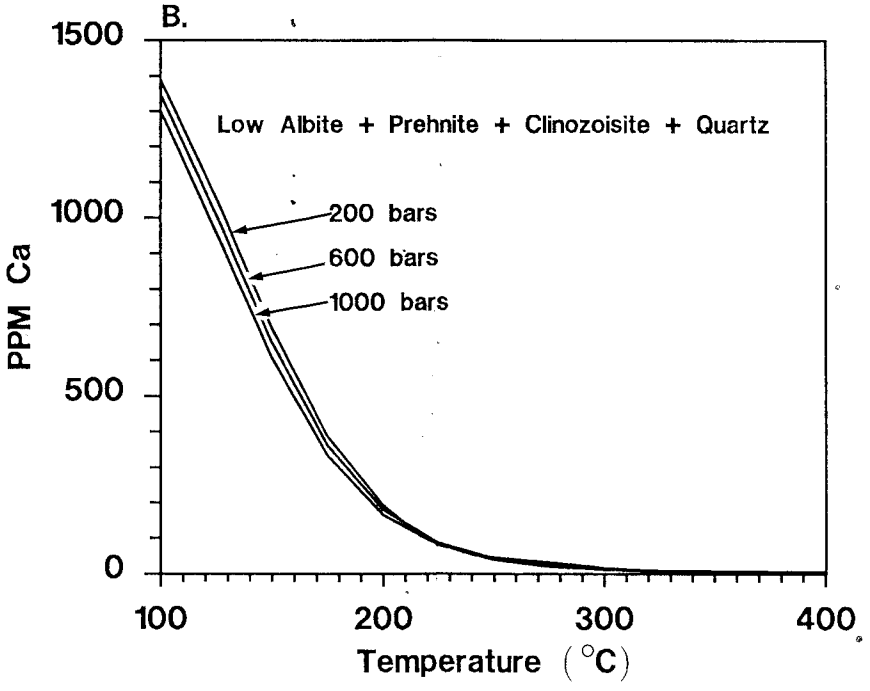
B.
1500
1000
500
0
PPM Ca
Low Albite + Prehnite + Clinozoisite + Quartz
200 bars
600 bars
1000 bars
100
200
300
400
Temperature (°C)

the required disequilibrium conditions can be provided by fluid flow along positive temperature gradients.

A number of authors have pointed out that fluid movement along positive temperature gradients will favor the precipitation of hydrous CaAl-silicates in hydrothermal systems (Hemley and others, 1971; Giggenbach, 1981, 1984, 1988; Rose and Bird, 1987; Berndt, Seyfried, and Janecky, 1989). In figure 14A calculated cation activity ratios $a_{Ca}/a^2_{Na^+}$ are shown as a function of temperature at pressures of 200, 600, and 1000 bars for local equilibrium among prehnite + clinozoisite + albite + quartz. These local equilibrium constraints require an increase in the activity of Na relative to Ca in the coexisting aqueous phase as temperature increases, which can be achieved by combined albite dissolution and CaAl-silicate precipitation.

Figure 14A provides little information on the absolute amount of Ca mass transfer associated with temperature or pressure variations. To evaluate this, one must account for aqueous activity coefficients and distribution of the various Ca species in the fluid phase. Results of a series of speciation-solubility calculations designed to assess these effects are given in figure 14B which shows the predicted change in Ca concentration in a 0.1 molal total chloride solution in equilibrium with albite, prehnite, clinozoisite, and quartz. The total Ca solubility is a sensitive function of temperature, but varying the pressure by 800 bars has only a very small effect. It would appear that temperature variations will have a much greater effect on Ca solubility than pressure variations in hydrothermal systems. For example, in the temperature range 200° to 250°C the change in Ca concentration in a fluid subjected to an overall temperature change of 5°C would, for an equivalent pressure effect, require a movement through a vertical distance of 3 km assuming a hydrostatic pressure head. The type and extent of metasomatism in geological systems is controlled by the derivatives of the curves that describe Ca-solubility in figure 14B and not by the absolute concentrations of components in solution. The largest extent of Ca mass transfer is expected to occur where fluids are moving through temperature intervals corresponding to large values for these derivatives.

Movement of fluids along positive temperature gradients will shift the ratio $a_{Ca^{2+}}/a^2_{Na^+}$ to values lower than those required for local equilibrium albite and CaAl-silicates. Systems that contain albite or $NaAlSi_3O_8$ component in plagioclase, will re-equilibriate along reaction paths similar

Fig. 14. (A) Phase relations in the system Na_2O–CaO–Al_2O_3–SiO_2–H_2O–HCl at 300°C between 200 and 1000 bars in equilibrium with quartz and an aqueous solution where $a_{H_2O} = 1$, expressed as the ratio log $a_{Ca^{2+}}/a^2_{Na^+}$ for local equilibrium between prehnite + clinozoisite + low-albite + quartz. (B) Total Ca concentration in a hydrothermal solution in local equilibrium with prehnite + clinozoisite + low-albite + quartz expressed as milligrams per kilogram as a function of temperature at 200, 600, and 1000 bars. Fluid compositions were calculated using the EQ3/6 computer code and assume a total Cl^- concentration of 0.1 m. Calculations below 500 bars at temperatures above 350°C should be regarded as approximate (Johnson, Oelkers, and Helgeson, 1991).

to those examined in these experiments. The importance of this process is evident from petrological examination of Ca-metasomatized rocks from East Greenland described earlier. These regions show a clear paragenesis between the early formation of albite and its subsequent replacement by CaAl-silicate phases (fig. 1).

CONCLUSIONS

Experimental observations during the irreversible hydrolysis of albite in aqueous solutions that satisfy local equilibrium with wairakite, prehnite, and quartz suggest there is close agreement between observed and predicted reaction paths. After initial changes in fluid composition caused by progressive saturation of intermediate phases, the reaction is characterized by coupled Na and Ca exchange related to the dissolution of albite and the concomitant precipitation of wairakite; at a late stage of reaction this process is replaced by a concomitant addition of Na and Al to solution without Ca removal indicating that Al dissolves to form $Al(OH)_4^-$. These processes are related via the mass and charge balance constraints of the system and by the buffering of the $a_{Ca^{2+}}/a_{H^+}^2$ ratio in the fluid by coexisting prehnite and wairakite.

Integrated over time, the reaction examined in these experiments represents an analog to Ca-metasomatism in natural systems. In the experimental closed system, the extent of Ca metasomatism is small because albite soon reaches equilibrium at which point the driving force for the reaction is removed. However, in open systems in the presence of temperature, pressure, or compositional gradients, disequilibrium conditions may be maintained for periods long enough for substantial elemental mass transfer to occur. Analysis of the temperature dependence of solubilities and stabilities of CaAl-silicate and albite suggests that Ca-metasomatism is likely to be a consequence of fluids moving up temperature gradients, possibly associated with fluids moving laterally toward heat sources in the deeper portions of hydrothermal systems.

Theoretical mass transfer calculations provide useful guidelines for optimizing run conditions for solubility and water-rock experiments. Examined within a simple chemical and mineralogical system, the combination of theoretical modeling and experimental observation allows for identification of specific mineral-fluid reactions that control the evolution of the system.

ACKNOWLEDGMENTS

This study represents part of the senior author's Ph.D. thesis at Stanford University. We are grateful to a number of people who have offered advice or practical help during the course of these experiments including Jonathan Stebbins, Heather Boek, Jared Potter, Craig Manning, Eric Winterburn, and Paul Birch. The albite starting material used in this study was obtained from Bob Coleman. We would like to thank Ken Jackson, Bill Bourcier, and James Johnson for advice concerning the use of EQ3/6 and its database. An early review of this manuscript by John

Apps and two anonymous reviewers has resulted in significant improvements. This research was supported by the National Science Foundation: NSF-EAR 85-07988 (to J. G. Liou); NSF-EAR 86-06256 and NSF-EAR 88-03754 (to D. K. Bird).

References

Balsillie, D., 1932, The Ballantrae igneous complex, South Ayrshire: Geological Magazine, v. 69, p. 107–131.

Berndt, M. E., Seyfried, W. E., Jr., and Janecky, D. R., 1989, Plagioclase and epidote buffering of cation ratios in mid-ocean ridge hydrothermal fluids: Experimental results in and near the supercritical region: Geochimica et Cosmochimica Acta, v. 53, p. 2283–2301.

Bird, D. K., Manning, C. E., and Rose, N. M., 1988, Hydrothermal alteration of Tertiary layered gabbros, East Greenland: American Journal of Science, v. 288, p. 405–457.

Bird, D. K., Rosing, M. T., Manning, C. E., and Rose, N. M., 1985, Geologic field studies of the Miki Fjord area, East Greenland: Bulletin of the Geological Society of Denmark, v. 34, p. 219–236.

Bird, D. K., Schiffman, P., Elders, W. A., Williams, A. E., and McDowell, S. D., 1984, Calcsilicate mineralization in active geothermal systems: Economic Geology, v. 79, p. 671–695.

Bourcier, W. L., Knauss, K. G., and Jackson, K. J., 1987, Aluminum hydrolysis constants to 250°C determined from boehmite solubility measurements: Geological Society of America, Abstracts with Programs, v. 19, p. 596.

Cho, M., and Liou, J. G., 1987, Prehnite-pumpellyite to greenschist facies transition in the Karmutsen metabasites, Vancouver Island, British Columbia: Journal of Petrology, v. 28, p. 417–443.

De Donder, Th., and Van Rysselberghe, P., 1936, The thermodynamic theory of affinity: Stanford University Press.

Donnay, J. D. H., and Ondik, H. M., 1973, Crystal data determinative tables, 3d ed: U.S. Dept. Commerce, National Bureau of Standards, Joint Committee on Powder Diffraction Standards, v. 2, p. 1580 pp.

Fournier, R. O., and Potter, R. W., 1982, An equation correlating the solubility of quartz in water from 25°C to 900°C at pressures up to 10,000 bars: Geochimica et Cosmochimica Acta, v. 46, p. 1969–1973.

Giggenbach, W. F., 1981, Geothermal mineral equilibria: Geochimica et Cosmochimica Acta, v. 45, p. 393–410.

———— 1984, Mass transfer in hydrothermal alteration systems: Geochimica et Cosmochimica Acta, v. 48, p. 2693–2711.

———— 1988, Geothermal solute equilibria. Derivation of the Na-K-Mg-Ca geoindicators: Geochimica et Cosmochimica Acta, v. 52, p. 2749–2767.

Harper, G. D., Bowman, J. R., and Kuhns, R., 1988, Field, chemical and isotopic aspects of subseafloor metamorphism of the Josephine Ophiolite, California-Oregon: Journal of Geophysical Research, v. 93, p. 4625–4657.

Harrigan, D. B., and Maclean, W. H., 1976, Petrography and geochemistry of epidote alteration patches in gabbro dykes at Matagami, Quebec: Canadian Journal of Earth Science, v. 13, p. 500–511.

Helgeson, H. C., 1968a, Evaluation of irreversible reactions in geochemical processes involving minerals and aqueous solutions I. Thermodynamic relations: Geochimica et Cosmochimica Acta, v. 32, p. 853–877.

———— 1969, Thermodynamics of hydrothermal systems at elevated temperatures and pressures: American Journal of Science, v. 267, p. 729–804.

———— 1970, Description and interpretation of phase relations in geochemical processes involving aqueous solutions: American Journal of Science, v. 268, p. 415–438.

———— 1979, Mass transfer among minerals and hydrothermal solutions, *in* Barnes, H. L., editor, Geochemistry of hydrothermal ore deposits: New York, John Wiley & Sons, p. 568–606.

Helgeson, H. C., Brown, T. H., Nigrini, A., and Jones, T. A., 1970, Calculation of mass transfer in geothermal processes involving aqueous solutions: Geochimica et Cosmochimica Acta, v. 34, p. 569–592.

Helgeson, H. C., Delany, J. M., Nesbitt, H. W., and Bird, D. K., 1978, Summary and critique of the thermodynamic properties of rock-forming minerals: American Journal of Science, v. 278-A, 229 pp.

Helgeson, H. C., and Kirkham, D. H., 1974, Theoretical prediction of the thermodynamic behavior of aqueous electrolytes at high pressures and temperatures: I. Summary of the thermodynamic properties of the solvent: American Journal of Science, v. 274, p. 1089–1198.

Helgeson, H. C., Kirkman, D. H., and Flowers, G. C. 1981, Theoretical prediction of the thermodynamic properties of aqueous electrolytes at high pressures and temperatures: IV. Calculation of activity coefficients, osmotic coefficients, and apparent molal and standard and relative partial molal properties to 600°C and 5KB: American Journal of Science, v. 281, p. 1249–1516.

Helgeson, H. C., Murphy, W. M., and Aagaard, P., 1984, Thermodynamic and kinetic constraints on reaction rates among minerals and aqueous solutions. II. Rate constants, effective surface area, and the hydrolysis of feldspar: Geochimica et Cosmochimica Acta, v. 48, p. 2405–2432.

Hemley, J. J., Montoya, J. W., Nigrini, A., and Vincent, H. A., 1971, Some alteration reactions in the system CaO-Al_2O_3-SiO_2-H_2O: Society of Mining Geology of Japan, Special Issue 2, p. 58–63.

Johnson, J. W., Oelkers, E. H., and Helgeson, H. C., 1992, SUPCRT 92: A software package for calculating the standard modal thermodynamic properties of minerals, gases, aqueous species, and reactions from 1 to 5000 bars and 0° to 1000°C: Computers and Geosciences, in press.

Knauss, K. G., and Wolery, T. J., 1986, Dependence of albite dissolution on pH and time at 25°C and 70°C: Geochimica et Cosmochimica Acta, v. 50, p. 2481–2497.

Liou, J. G., Maruyama, S., and Cho, M., 1985, Phase equilibria and mineral paragenesis in low-grade metamorphism: Mineralogical Magazine, v. 49, p. 321–333.

Marzouki, F., Kerrich, R., and Fyfe, W. S., 1979, Epidotisation of diorites at Al Haddah, Saudi Arabia: Fluid influx into cooling plutons: Contributions to Mineralogy and Petrology, v. 68, p. 281–284.

Richardson, C. J., Cann, J. R., Richards, H. G., and Cowan, J. G., 1987, Metal-depleted root zones of the Troodos ore-forming hydrothermal systems, Cyprus: Earth and Planetary Science Letters, v. 84, p. 243–253.

Rose, N. M., ms, 1990, Geochemistry of hydrothermal metasomatism in basaltic systems: Ph.D. thesis, Stanford University, 232 p.

Rose, N. M., and Bird, D. K., 1987, Prehnite–epidote phase relations in the Nordre Aputitêq and Kruuse Fjord layered gabbros, East Greenland: Journal of Petrology, v. 28, p. 1193–1218.

———— 1990, A model for metasomatism in basic dikes. V. M. Goldschmidt Conference, Programs and Abstracts, Baltimore, MD.

Schiffman, P., Bettison, L. A., and Smith, B. M., 1990, Mineralogy and geochemistry of epidosites from the Solea Graben, Troodos ophiolite, Cyprus, *in* Malpas, J., Moores, E. M., Panayiotou, A., and Xenophontos, C., editors, Ophiolites, Oceanic Crustal Analogues, proceedings of the symposium 'Troodos 1987,' p. 673–683.

Schiffman, P., and Smith, B. M., 1988, Petrology and oxygen isotope geochemistry of a fossil seawater hydrothermal system within the Solea Graben, northern Troodos Ophiolite, Cyprus: Journal of Geophysical Research, v. 93, p. 4612–4624.

Schiffman, P., Smith, B. M., Vargas, R. J., and Moores, E. M., 1987, Geometry, conditions, and timing of off-axis hydrothermal metamorphism and ore deposition in the Solea graben, N. Troodos ophiolite, Cyprus: Nature, v. 325, p. 423–425.

Seyfried, W. E., Janecky, D. R., and Berndt, M. E., 1987, Rocking autoclaves for hydrothermal experiments II. The flexible reaction-cell system, *in* Ulmer, G. C., and Barnes, H. L., editors, Hydrothermal Experimental Techniques: New York, John Wiley & Sons, p. 216–240.

Shock, E. L., and Helgeson, H. C., 1988, Calculation of the thermodynamic and transport properties of aqueous species at high pressures and temperatures: Correlation algorithms for ionic species and equation of state predictions to 5 kb and 1000 C: Geochimica et Cosmochimica Acta, v. 52, p. 2009–2036.

Shock, E. L., Helgeson, H. C., and Sverjensky, D. A., 1989, Calculation of the thermodynamic and transport properties of aqueous species at high pressures and temperatures: Standard partial molal properties of inorganic neutral species: Geochimica et Cosmochimica Acta, v. 53, p. 2157–2183.

Sverjensky, D. A., Hemley, J. J., and d'Angelo, W. M., 1991, Thermodynamic assessment of hydrothermal alkali feldspar-mica-aluminosilicate equilibria: Geochimica et Cosmochimica Acta, v. 55, p. 989–1004.

Tanger, J. C., and Helgeson, H. C., 1988, Calculation of the thermodynamic and transport properties of aqueous species at high pressures and temperatures: Revised equation of state for the standard partial molal properties of ions and electrolytes: American Journal of Science, v. 288, p. 19–98.

Thompson, J. B., Jr., Waldbaum, D. R., and Hovis, G. L., 1974, Thermodynamic properties related to ordering in end-member alkali feldspars, *in* Mackenzie, W. S., and Zussman, J., editors, The Feldspars: New York, Crane, Russak and Co. Inc., p. 218–248.

Walther, J. V., and Helgeson, H. C., 1977, Calculation of the thermodynamic properties of aqueous silica and the solubility of quartz and its polymorphs at high pressures and its polymorphs at high pressures and temperatures: American Journal of Science, v. 277, p. 1315–1351.

Watson, K. D., 1953, Prehnitization of albitite. American Mineralogist, v. 38, p. 197–205.

Wolery, T. J., 1979, Calculation of chemical equilibrium between aqueous solutions and minerals: the EQ3/6 software package: UCRL-52658, Lawrence Livermore Laboratory.

———— 1983, EQ3NR, a computer program for geochemical aqueous speciation-solubility calculations: User's guide and documentation: UCRL-53414, Lawrence Livermore Laboratory.